© 2021. Published by The Company of Biologists Ltd | Journal of Cell Science (2021) 134, jcs258462. doi:10.1242/jcs.258462

RESEARCH ARTICLE

The Bardet–Biedl syndrome complex component BBS1 controls T cell polarity during immune synapse assembly

Chiara Cassioli[1], Anna Onnis[1], Francesca Finetti[1], Nagaja Capitani[1], Jlenia Brunetti[2], Ewoud B. Compeer[3], Veronika Niederlova[4], Ondrej Stepanek[4], Michael L. Dustin[3] and Cosima T. Baldari[1,*]

ABSTRACT

Components of the intraflagellar transport (IFT) system that regulates the assembly of the primary cilium are co-opted by the non-ciliated T cell to orchestrate polarized endosome recycling and to sustain signaling during immune synapse formation. Here, we investigated the potential role of Bardet–Biedl syndrome 1 protein (BBS1), an essential core component of the BBS complex that cooperates with the IFT system in ciliary protein trafficking, in the assembly of the T cell synapse. We demonstrated that BBS1 allows for centrosome polarization towards the immune synapse. This function is achieved through the clearance of centrosomal F-actin and its positive regulator WASH1 (also known as WASHC1), a process that we demonstrated to be dependent on the proteasome. We show that BBS1 regulates this process by coupling the 19S proteasome regulatory subunit to the microtubule motor dynein for its transport to the centrosome. Our data identify the ciliopathy-related protein BBS1 as a new player in T cell synapse assembly that functions upstream of the IFT system to set the stage for polarized vesicular trafficking and sustained signaling.

This article has an associated First Person interview with the first author of the paper.

KEY WORDS: Immune synapse, Primary cilium, Bardet–Biedl syndrome, Centrosome, Proteasome, Dynein

INTRODUCTION

Vesicular trafficking has emerged over recent years as a central factor in the assembly and function of the immune synapse (IS), a specialized membrane domain that T cells form at the interface with antigen-presenting cells (APCs) carrying specific major histocompatibility complex (MHC)-bound peptide antigen (Dustin, 2014). Essential components of the T cell receptor (TCR) signaling cascade are present as two pools with different and dynamic subcellular localization. These include the TCR itself, the initiating kinase LCK and the transmembrane adaptor LAT, which couples TCR engagement to multiple intracellular signaling modules (Ehrlich et al., 2002; Bonello et al., 2004; Das et al., 2004). One pool is associated to the plasma membrane and is readily mobilized upon TCR triggering to orchestrate the signals that initiate the topological reorganization of receptors and signaling mediators leading to the generation of the mature IS architecture. The second pool is associated to recycling endosomes, which undergo polarized exocytosis at the IS following centrosome translocation towards the T cell–APC interface to sustain signaling (Soares et al., 2013; Finetti et al., 2017; Onnis and Baldari, 2019). Vesicular trafficking also regulates the fate of exhausted TCRs, which accumulate at the IS center and undergo endocytosis to be sorted for recycling or lysosome-mediated degradation (Vardhana et al., 2010; Alcover et al., 2018; Compeer et al., 2018). Moreover, post-endocytic TCRs are exploited for intercellular communication through their incorporation into synaptic ectosomes that are released into the synaptic cleft to be taken up by the cognate APC (Choudhuri et al., 2014).

Accumulating evidence for a crucial role of membrane trafficking in IS assembly and function has placed the focus on the characterization of the underlying molecular machinery. We have previously identified the intraflagellar transport (IFT) system as an unexpected new player in synaptic trafficking (Finetti et al., 2009, 2014; Galgano et al., 2017). This multimolecular complex, consisting of the IFT-A and IFT-B subcomplexes, regulates the growth, disassembly and signaling function of the primary cilium, a small appendage present on the majority of mammalian cells, a major exception being hematopoietic cells (Pedersen and Rosenbaum, 2008). We found that IFT20 promotes IS assembly together with other IFT-B components by regulating polarized TCR recycling in the non-ciliated T cell (Finetti et al., 2009, 2014; Galgano et al., 2017). Many other ciliary proteins have since been demonstrated to be co-opted by T cells for IS formation, including adaptors [e.g. Unc119, the Rab11 family-interacting protein FIP3 (also known as RAB11FIP3) and the microtubule-binding protein EB-1 (encoded by *MAPRE1*)], small GTPases [e.g. Rab8a and Rab8b, Rab7l1 (also known as Rab29), Arl3 and Arl13b (also known Arl2l1)] and tethering proteins [e.g. the SNAREs VAMP3 and VAMP7, and the golgin GMAP210 (also known as TRIP11)] (Das et al., 2004; Martín-Cófreces et al., 2012; Larghi et al., 2013; Finetti et al., 2015; Onnis et al., 2015; Bouchet et al., 2016; Stephen et al., 2018; Zucchetti et al., 2019). Additionally, ciliary signaling pathways, such as Hedgehog, and lipid kinase and phosphatase networks, are exploited by cytotoxic T cells (CTLs) for the assembly of the lytic synapse (de la Roche et al., 2013; Gawden-Bone et al., 2018), leading to the hypothesis that the IS and the primary cilium are functional homologs (Baldari and Rosenbaum, 2010; de la Roche et al., 2016; Cassioli and Baldari, 2019).

Here, we have investigated the potential role of the Bardet–Biedl syndrome complex or BBSome, a key regulator of ciliary function that interacts functionally and physically with IFT-B, in IS assembly. The BBSome is an octameric, centrosome-associated complex that undergoes IFT and is responsible for retrieving

[1]Department of Life Sciences, University of Siena, 53100, Siena, Italy. [2]Department of Medical Biotechnologies, University of Siena, 53100, Siena, Italy. [3]Kennedy Institute of Rheumatology, University of Oxford, OX3 7FY, Oxford, UK. [4]Institute of Molecular Genetics of the Czech Academy of Sciences, 142 20, Prague, Czech Republic.

*Author for correspondence (baldari@unisi.it)

C.C., 0000-0002-4853-2298; A.O., 0000-0003-3199-9868; N.C., 0000-0003-3653-8972; J.B., 0000-0001-8144-7186; E.B.C., 0000-0002-3050-7633; O.S., 0000-0002-2735-3311; M.L.D., 0000-0003-4983-6389; C.T.B., 0000-0002-4414-6744

Handling Editor: Daniel Billadeau
Received 26 January 2021; Accepted 6 July 2021

Journal of Cell Science

Journal of Cell Science (2021) 134, jcs258462. doi:10.1242/jcs.258462

membrane cargoes, such as activated G-protein-coupled receptors (GPCRs), at the tip of the cilium, where it assembles with IFT-B to promote their exit from the cilium by regulating their passage through the diffusion barrier at the ciliary base (Nachury, 2018; Nakayama and Katoh, 2018). We show that the BBSome core component Bardet–Biedl syndrome 1 protein (BBS1) (Mourão et al., 2014) is essential for centrosome translocation towards the T cell interface with cognate APC. We provide evidence that BBS1 promotes proteasome-dependent F-actin clearance around the centrosome, on which its mobilization to the IS crucially depends. We also show that BBS1 regulates this process by coupling the 19S regulatory subunit of the proteasome to the microtubule motor dynein for its transport to the centrosome. Collectively, our data identify the ciliopathy-related protein BBS1 as a new player in the assembly of the T cell IS that functions upstream of the IFT system to set the stage for polarized recycling and sustained signaling.

RESULTS

BBS1 localizes at the pericentrosomal compartment and accumulates at the T cell IS

To investigate the role of the BBSome in IS assembly in human T cells, we first measured the expression of its eight core components [*BBS1*, *BBS2*, *BBS4*, *BBS5*, *BBS7* (also known as *BBS2L1*), *BBS8* (also known as *TTC8*), *BBS9* (also known as *PTHB1*) and *BBS18* (also known as *BBIP1*)] in both Jurkat and primary peripheral blood T cells, using the ciliated fibroblast line BJ-5ta as a positive control. Expression was comparable or higher in primary T cells compared to ciliated cells with the exception of BBS8, as assessed by reverse transcription-quantitative PCR (RT-qPCR) (Fig. S1A). Jurkat cells also expressed all core BBSome components, albeit at levels lower than primary T cells (Fig. S1A). T cell expression was confirmed by immunoblotting for BBS1 (Fig. 1A), which we chose for further characterization as it is essential for recruitment of GTP-bound BBS3 (also known as Arl6) to the BBSome to enable its entry into the cilium (Mourão et al., 2014) and contributes to BBSome stability (Prasai et al., 2020). Of note, the protein levels of BBS1 were higher in Jurkat cells compared to primary T cells, despite their lower mRNA abundance, which might reflect higher protein stability in the former.

The subcellular localization of BBS1 was determined by confocal immunofluorescence analysis of Jurkat cells transfected with GFP-tagged BBS1 (BBS1–GFP) and co-stained with markers of intracellular compartments. Since the BBSome is localized at the basal body in ciliated cells (Nachury, 2018; Wingfield et al., 2018), for this analysis we chose markers of the centrosome (γ-tubulin) and of the pericentrosomal [PCM1, CEP131 (also known as AZI1) and CEP290] and endocytic recycling (Rab11a) compartments. Markers of the Golgi complex (GM130, encoded by *GOLGA2*) and late endosomes (Rab7a) were also included. Similar to ciliated cells, BBS1 colocalized most prominently with the centrosomal and pericentrosomal compartments, and with recycling endosomes (Fig. 1B,C; Fig. S2A).

During IS formation the centrosome moves towards the APC, allowing for polarized delivery to the synaptic membrane of a pool of TCR–CD3 complexes associated with recycling endosomes (Soares et al., 2013; Onnis and Baldari, 2019). BBS1 polarized to the IS formed in conjugates of Jurkat cells to Raji cells (used as APCs) pulsed with staphylococcal enterotoxin E (SEE). At the IS, BBS1 colocalized with the centrosome and CD3ζ$^+$ endosomes (Fig. 1D). This result was confirmed in peripheral blood T cells purified from healthy donors and conjugated to Raji cells pulsed with a mix of superantigens (SAgs) including staphylococcal enterotoxin A (SEA), staphylococcal enterotoxin B (SEB) and SEE to cover a substantial proportion of the TCR Vβ repertoire and hence maximize the number of responding T cells (Fig. 1E). Of note, BBS4, which primes the assembly of a pre-BBSome complex in ciliated cells (Prasai et al., 2020), also polarized to the IS together with the centrosome (Fig. S1B), suggesting the hypothesis that other BBS proteins might participate in IS assembly.

BBS1 is required for centrosome translocation to the IS

The homology between the IS and the primary cilium (Baldari and Rosenbaum, 2010; de la Roche et al., 2016; Cassioli and Baldari, 2019) led us to hypothesize that BBS1, which is essential for ciliogenesis (Katsanis, 2004; Tobin and Beales, 2009), could participate in IS assembly. To address this question, we transduced Jurkat cells with lentiviral particles containing a BBS1-specific shRNA to generate a stable BBS1 knockdown (KD) cell line (J KD; 90% depletion). A non-targeting shRNA was used to generate a control line (ctr) (Fig. S3A, left panel). The analysis was extended to a CRISPR-Cas9-edited pool of primary T cells knocked out for BBS1 expression (T KO; ∼70% depletion) (Fig. S3A, middle panel). BBS1 depletion did not affect either the levels of surface CD3ε (Fig. S3B) or expression of the other BBSome core components (Fig. S3C).

A central event in IS assembly is centrosome repositioning towards the APC together with the Golgi complex and the endosomal recycling compartment (Soares et al., 2013; Bustos-Morán et al., 2016). This allows for the polarized transport to the IS not only of endosomal TCRs, but also of signaling mediators associated with recycling endosomes, including the kinase LCK (Ehrlich et al., 2002), the transmembrane adaptor LAT (Bonello et al., 2004) and the small GTPase Rac1 (Bouchet et al., 2016), all of which contribute to sustain signaling during T cell activation. Based on the centrosomal localization of BBS1, we addressed the outcome of BBS1 deficiency on centrosome translocation to the IS in 15 min conjugates, a time point when IS maturation has fully occurred. BBS1 depletion in either Jurkat or primary T cells resulted in defective centrosome polarization (Fig. 2A–E; Fig. S2B, Fig. S4A,B).

In many cell types, the centrosome is closely associated to the nuclear membrane, suggesting that the defect in centrosome translocation to the IS formed by BBS1-deficient T cells might be related to its inability to dissociate from the nucleus, as reported for B cells (Obino et al., 2016). To address this issue, the distance of the centrosome from the nuclear membrane was measured in SAg-specific conjugates of control and BBS1 knockout (KO) primary T cells co-stained for the centrosomal marker pericentrin (PCNT) and the linker of nucleoskeleton and cytoskeleton (LINC) complex component nesprin-2 (also known as Syne-2), which associates with the nuclear membrane (Burakov and Nadezhdina, 2013) (Fig. 2B,E; Fig. S4B,C for parameters used for quantification). The distance between the centrosome and the nuclear membrane increased in antigen-specific conjugates of control cells compared to conjugates formed in the absence of SAgs, concomitant with centrosome translocation to the IS (Fig. 2B,D,E; Fig. S4B). In contrast, no difference in the distance of the centrosome from the nuclear membrane could be observed in conjugates formed by BBS1 KO T cells in the absence or presence of SAgs (Fig. 2E; Fig. S4B). Consistent with the defect in centrosome repositioning to the IS, the accumulation of endosomal TCR–CD3 complexes at the IS was impaired in 15 min conjugates formed by BBS1-deficient T cells (Fig. 2F–I; Fig. S4A,D).

Since centrosome detachment from the nucleus has been shown to be dispensable in CD8$^+$ T cells (Lui-Roberts et al., 2012), we extended the analysis to control and BBS1 KO CD4$^+$ T cells (Fig. S5A).

Journal of Cell Science (2021) 134, jcs258462. doi:10.1242/jcs.258462

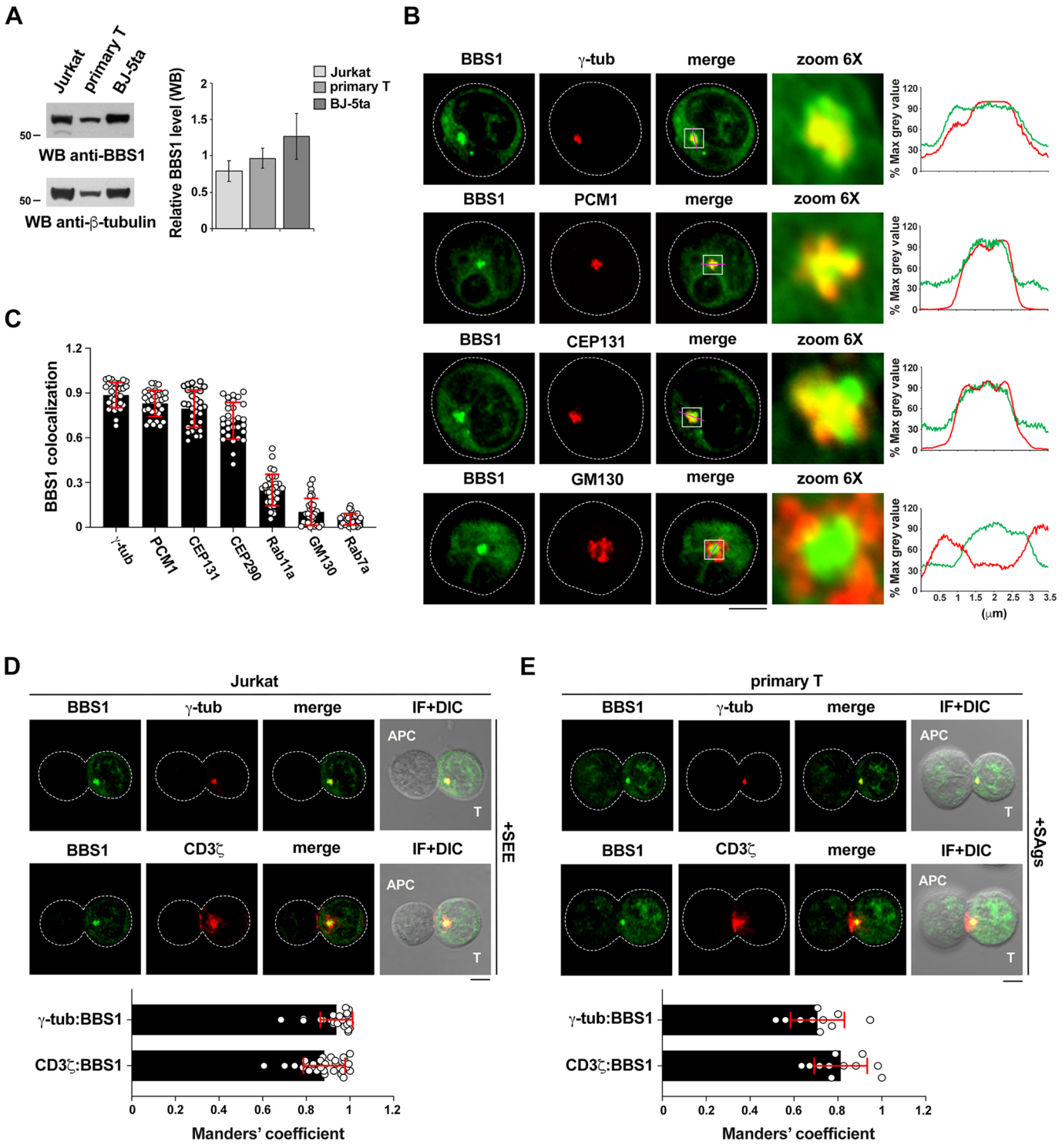

Fig. 1. BBS1 localizes at the pericentrosomal compartment and accumulates at the T cell IS. (A) Left: Immunoblot analysis of BBS1 in lysates of Jurkat, primary T and BJ-5ta cells ($n \geq 3$). The migration of molecular mass markers is shown (kDa). Right: Quantification (mean±s.d.) of the relative protein expression normalized to β-tubulin. WB, Western blot. (B) Immunofluorescence analysis of BBS1–GFP-expressing Jurkat cells co-stained for markers of different intracellular compartments. Representative images (medial optical sections) are shown. Dashed lines mark the cell outline. Boxes indicate regions shown in 6× zoom images. Right: Intensity profiles along the lines within the selected areas in the overlay images for each channel are shown. Raw pixel intensity signals were normalized to maximum intensity pixel of each channel (% max grey value). γ-tub, γ-tubulin. (C) Quantification (mean±s.d.) using Manders' coefficient of the weighted colocalization of each marker with GFP in stable or transient Jurkat BBS1–GFP transfectants (10 cells/sample, $n \geq 3$). Representative images (medial optical sections) are shown in B and Fig. S2A. (D,E) Immunofluorescence (IF) analysis of γ-tubulin and CD3ζ localization in Jurkat cells (D) or primary T cells (E) transfected with a construct encoding BBS1–GFP and conjugated with SEE-loaded (D) or SAg-loaded (E) Raji cells (APCs) for 15 min. Dashed lines mark the outline of the two cells. DIC, differential interference contrast. Bottom: Quantification (mean±s.d.) using Manders' coefficient of the weighted colocalization of the indicated markers with GFP. The distance of BBS1–GFP (μm) from the T cell–APC contact site, measured from the point of maximal intensity of the GFP signal, was 2.99±0.85 in Jurkat cells (mean±s.d.; 10 cells/sample, $n=3$) and 1.13±0.85 in primary T cells (≥10 cells, $n=2$). Scale bars: 5 μm.

Journal of Cell Science (2021) 134, jcs258462. doi:10.1242/jcs.258462

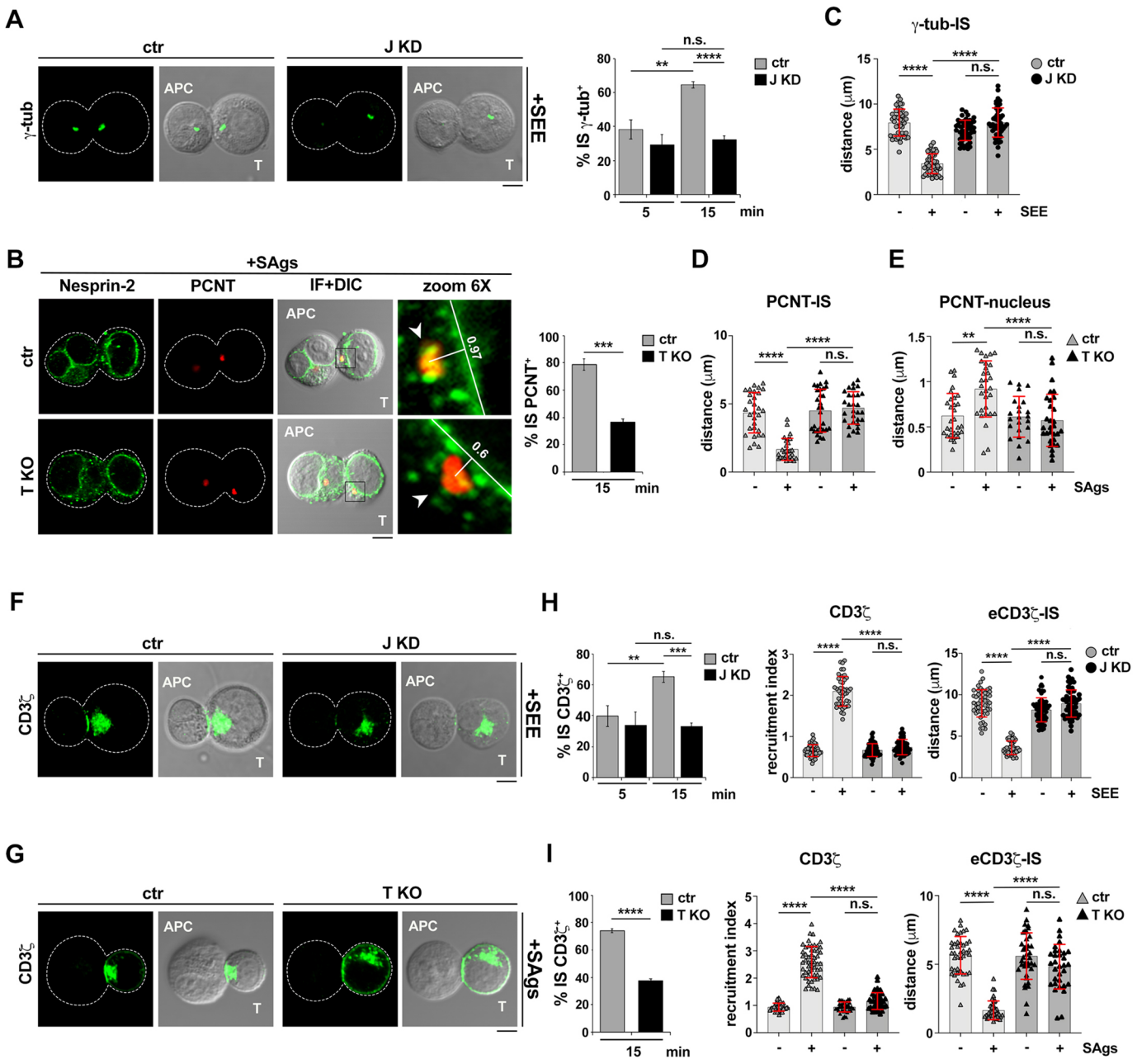

Fig. 2. BBS1 is required for centrosome and endosomal TCR translocation to the IS. (A,B) Immunofluorescence (IF) analysis of γ-tubulin (γ-tub) (A) or pericentrin (PCNT) (B) in conjugates of control (ctr) and BBS1 KD (J KD) Jurkat cells (A), or control (ctr) and BBS1 KO primary T cells (T KO) (B), with SEE- and SAgs (SEA+SEB+SEE)-loaded Raji cells (APCs), respectively. Conjugates were co-stained for nesprin-2 (B). Left: Representative images (medial optical sections) of conjugates formed in the presence of SEE or SAgs (see Fig. S4A,B for SEE- and SAg-independent conjugates). Boxes in B indicate the regions shown in 6× zoom images. Arrowheads in B indicate the centrosomes and the perpendicular lines show the centrosome-nucleus distances (see Fig. S4C for quantification). DIC, differential interference contrast. Right: Quantification (percentage) of antigen-specific conjugates harboring γ-tubulin (A) or PCNT (B) staining at the IS (≥25 cells/sample, *n*=3, unpaired two-tailed Student's *t*-test). (C,D) Measurement of the distance (μm) of the centrosome (γ-tubulin or PCNT) from the T cell–APC contact site in 15 min conjugates of control (ctr) and BBS1 KD (J KD) Jurkat cells (C), or control (ctr) and BBS1 KO primary T cells (T KO) (D), with Raji cells in the absence or presence of SEE (C) or SAgs (D) (≥10 cells/sample, *n*=3, Kruskal–Wallis test). (E) Measurement of the distance (μm) of the centrosome (PCNT) from the nuclear membrane (nesprin-2) in 15 min conjugates of control (ctr) and BBS1 KO (T KO) primary T cells with Raji cells in the absence or presence of SAgs (≥10 cells/sample, *n*=3, Kruskal–Wallis test). (F,G) Immunofluorescence (IF) analysis of CD3ζ in conjugates of control (ctr) and BBS1 KD (J KD) Jurkat (F), or control (ctr) and BBS1 KO primary T cells (T KO) (G), with SEE and SAg-loaded Raji cells (APCs). Representative images (medial optical sections) of the conjugates formed in the presence of SEE or SAgs are shown (see Fig. S4A,D for SEE- and SAg-independent conjugates). (H,I) Left: Quantification (percentage) of antigen-specific conjugates harboring CD3ζ staining at the IS (≥25 cells/sample, *n*=3, unpaired two-tailed Student's *t*-test). Middle: Relative CD3ζ fluorescence intensity at the IS in 15 min conjugates of control (ctr) and BBS1 KD (J KD) Jurkat cells (H), or control (ctr) and BBS1 KO primary T cells (T KO) (I), with SEE- and SAg-loaded Raji cells (≥10 cells/sample, *n*=3, Kruskal–Wallis test). Right: Measurement of the distance (μm) of the endosomal TCR–CD3 pool (eCD3ζ) from the T cell–APC contact site in 15 min conjugates of control (ctr) and BBS1 KD (J KD) Jurkat cells (H), or control (ctr) and BBS1 KO primary T cells (T KO) (I), with Raji cells in the absence or presence of SEE or SAgs (≥10 cells/sample, *n*=3, Kruskal–Wallis test). Scale bars: 5 μm. Dashed lines in A,B,F,G indicate cell outlines. Data are expressed as mean±s.d. ****$P \leq 0.0001$; ***$P \leq 0.001$; **$P \leq 0.01$; n.s., not significant.

Journal of Cell Science (2021) 134, jcs258462. doi:10.1242/jcs.258462

BBS1 deficiency resulted in a failure of the centrosome to polarize towards the IS formed by $CD4^+$ T cells (Fig. S5B–D). Similar to Jurkat cells (derived from $CD4^+$ T cells) and total primary T cells (of which ∼70% were $CD4^+$; data not shown), an increase in the distance of the centrosome from the nuclear membrane was observed in control SAg-specific conjugates, whereas no difference was observed in their BBS1 KO counterparts (Fig. S5E), indicating that the centrosome moves away from the nucleus in $CD4^+$ T cells (Lui-Roberts et al., 2012), unlike in $CD8^+$ T cells, and that this process is BBS1 dependent. Hence BBS1 is required for centrosome dissociation from the nucleus and translocation towards the APC in $CD4^+$ T cells.

Centrosome repositioning is a rapid process that occurs within minutes after APC contact and is triggered by TCR engagement (Bustos-Morán et al., 2016). To understand whether the defect in centrosome polarization to the IS formed by BBS1-deficient T cells is the consequence of impaired TCR signaling, we measured synaptic phosphotyrosine (p-Tyr) signaling at an early (5 min) and late (15 min) time point following conjugate formation. Normal tyrosine phosphoprotein enrichment at the T cell interface with the APC was observed in 5 min antigen-specific conjugates formed by BBS1 KD Jurkat cells or BBS1 KO primary T cells. Conversely, p-Tyr signaling was impaired at the 15 min time point (Fig. 3A,B; Fig. S4A,D). This suggests that the signaling events triggered by the membrane-associated TCR–CD3 pool that eventually lead to centrosome translocation were initiated normally, but were not sustained in the absence of BBS1.

To further address this point, we measured the synaptic accumulation of two components of the TCR signaling cascade, namely the initiating kinase ZAP-70 and the transmembrane adaptor LAT, in SEE-specific conjugates formed by control and BBS1 KD cells, using antibodies that recognize the respective active form. Similar to total tyrosine phosphoproteins, IS accumulation of active ZAP-70 and LAT was comparable at an early time point (5 min), whereas it declined at a later time point (15 min) in BBS1 KD but not control cells (Fig. 3C,D; Fig. S4E,F). Additionally, the defect in sustained p-Tyr signaling in BBS1 KD cells was confirmed by flow cytometric analysis of protein tyrosine phosphorylation in T cells activated at different time points with SEE-pulsed APCs (Fig. 3E). Taken together, these results indicate that BBS1 is not required for early TCR signaling, on which centrosome polarization depends, ruling out a signaling defect as the cause of the failure of the centrosome to translocate to the IS in BBS1-deficient cells. Hence BBS1 participates in IS assembly by promoting the translocation of the centrosome towards the APC, which sets the basis for polarized TCR recycling to sustain signaling.

To understand whether the IS formation defects in BBS1 KD cells were causally linked to BBS1 deficiency, we generated a BBS1 knockout Jurkat line (J KO) by CRISPR-Cas9 gene editing (Fig. S3A, right panel). These cells recapitulated the IS defects observed in BBS1 KD cells (Fig. 3F). Restoring BBS1 expression in BBS1 KO cells by transfection with a construct encoding BBS1–GFP (Fig. S3D,E) rescued their ability to promote the synaptic polarization of the centrosome and endosomal TCRs in addition to local tyrosine phosphoprotein accumulation (Fig. 3F). Hence, BBS1 is required for the assembly of functional T cell synapses.

BBS1 is required for centrosomal F-actin clearance during IS formation

F-actin clearance from the centrosomal area has been recently shown to occur during IS formation in lymphocytes, allowing for centrosome polarization (Obino et al., 2016; Bello-Gamboa et al., 2020). Conjugate staining with fluorochrome-labelled phalloidin and anti-γ-tubulin antibodies revealed the expected synaptic polymerization of F-actin (Roy and Burkhardt, 2018) (Figs 4A and 5A–D; Fig. S4G,H) and the presence of a centrosomal F-actin pool tightly surrounded by a radial pattern of $F\text{-actin}^+$ dots (Fig. 4A). A colocalization analysis carried out on a 4.5 µm diameter region around the centrosome showed that these corresponded largely to early endosomes ($Rab5^+$), where actin is known to polymerize to promote recycling (Seaman et al., 2013), and to a lesser extent to recycling endosomes ($Rab11a^+$) (Fig. 5E,F).

To investigate the outcome of BBS1 deficiency on centrosomal F-actin clearance, we co-stained conjugates for F-actin and PCNT and carried out a colocalization analysis on a 2 µm diameter region that included only the centrosome, thus excluding the endosomal F-actin pool (see Fig. S4C for mask generation). In agreement with a previous report (Bello-Gamboa et al., 2020), centrosomal F-actin was found to decrease in SEE-specific conjugates of control Jurkat cells compared to conjugates formed in the absence of SEE. Conversely, the centrosomal F-actin pool did not change in SEE-specific conjugates formed by BBS1 KD cells (Fig. 4A,B upper graph). Similar results were obtained using either primary control and BBS1 KO T cells (Fig. 4B, lower graph), or their primary $CD4^+$ counterparts (Fig. S5F).

As opposed to centrosomal F-actin, endosomal F-actin was comparable between control and BBS1 KD cells, and no change was observed in response to SEE stimulation, as assessed by analyzing F-actin colocalization with Rab5 and Rab11a on individual endosomes (Fig. 5E,F). These results were confirmed in conjugates triple-stained for PCNT, Rab5 and F-actin, using a mask to exclude the centrosomal F-actin pool for the colocalization analysis (Fig. S6A,B; see Fig. S4C for mask generation). No effect of BBS1 deficiency was observed on F-actin polymerization at the IS, as assessed by quantification of phalloidin-stained cells (Fig. 5A,C; Fig. S4G). This was confirmed by quantifying synaptic F-actin in control and BBS1 KD Jurkat cells transiently transfected with the F-actin reporter mApple–LifeAct-7, which allowed exclusion of the F-actin signal of the APC at the T cell contact (Fig. 5B,D; Fig. S4H).

The WASH complex, which is an actin regulator, has been shown to promote F-actin accumulation around the centrosome by recruiting the branched F-actin nucleator Arp2/3 (Gomez and Billadeau, 2009; Farina et al., 2016; Obino et al., 2016). Since WASH is also associated with endosomes (Wang et al., 2018), we restricted the analyses to a 2 µm diameter region around the centrosome, as described above for F-actin (see Fig. S4C for mask generation). Colocalization analyses in control conjugates co-stained with anti-WASH1 (also known as WASHC1) and anti-γ-tubulin antibodies confirmed the presence in T cells of a centrosomal WASH1 (hereafter WASH) pool that decreased in antigen-specific conjugates formed by control but not BBS1-deficient T cells (Fig. 4C,D). Conversely, the endosomal WASH pool did not undergo significant changes in response to stimulation and was not affected by BBS1 deficiency, as assessed in conjugates co-stained for WASH and Rab5 or Rab11a (Fig. S6C,D). This could be accounted for by the fact that during IS formation WASH-dependent F-actin polymerization can be limited to the subpopulation of endosomes carrying receptors and signaling mediators that undergo polarized recycling and occurs over an extended time frame, as opposed to centrosomal F-actin. Interestingly, more WASH co-immunoprecipitated with γ-tubulin in BBS1 KD cells compared to controls (Fig. 4E), suggesting that WASH association with the centrosome is negatively regulated by BBS1. Collectively, these results indicate that BBS1 deficiency results in the failure of T cells to clear F-actin from the centrosomal area, concomitant with the

Journal of Cell Science (2021) 134, jcs258462. doi:10.1242/jcs.258462

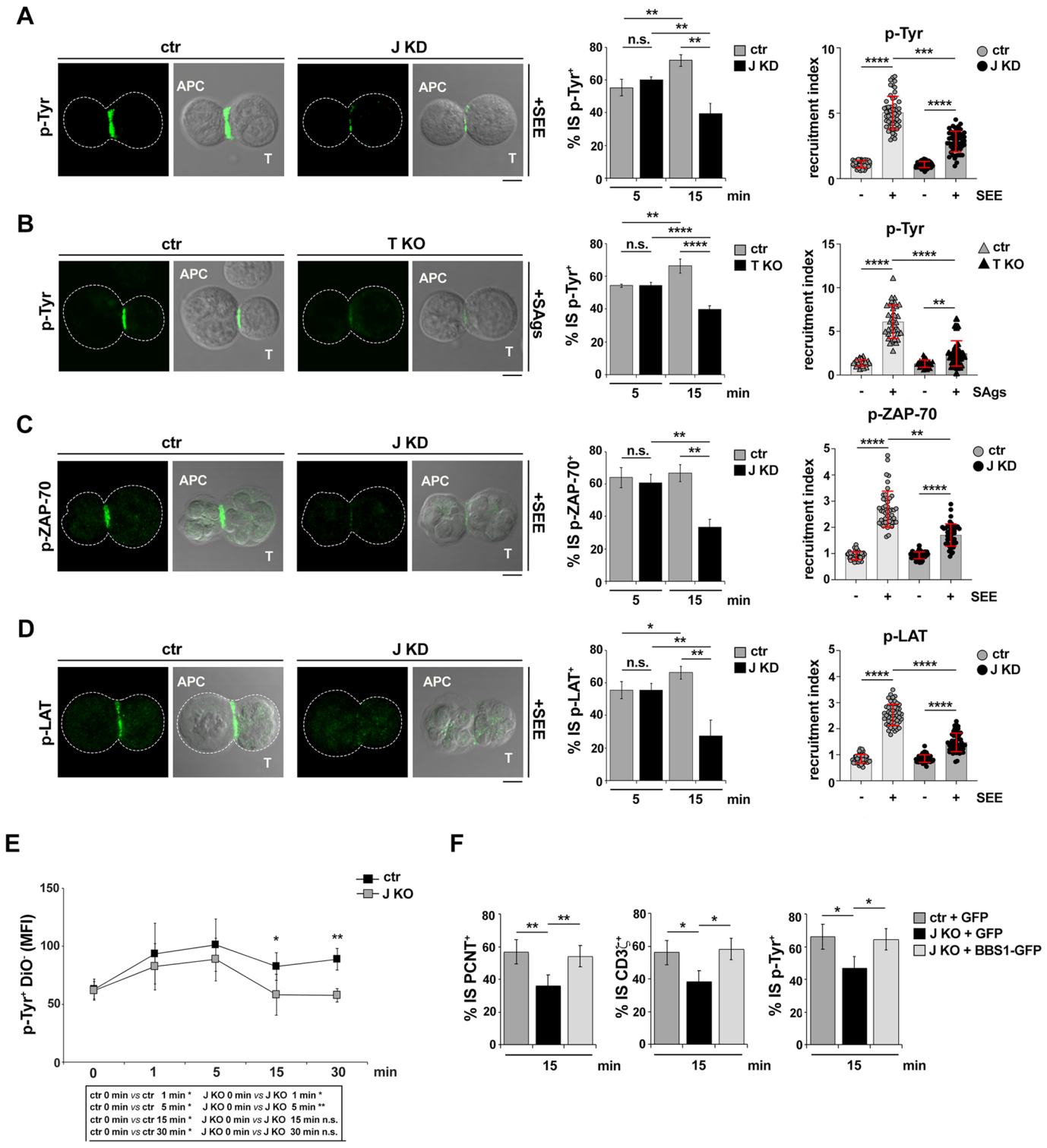

Fig. 3. See next page for legend.

persistence of the centrosomal WASH pool that sustains the polymerization of new actin filaments, which might account for the inability of the centrosome to translocate to the IS.

Centrosome translocation to the IS is regulated by the proteasome

The composition and function of the centrosome is dynamically regulated by a local proteasome pool that fine-tunes the concentration of cell cycle regulators, cell fate determinants and other mediators of key cellular processes in a variety of cell types, including immune cells (Vora and Phillips, 2016). Interestingly, proteasome activity has been implicated in F-actin remodeling at the centrosome to allow for its dissociation from the nucleus and translocation to the IS in B cells (Ibañez-Vega et al., 2019).

To assess the role of the proteasome in F-actin clearance around the centrosome and its translocation towards the T cell IS, we

Journal of Cell Science (2021) 134, jcs258462. doi:10.1242/jcs.258462

Fig. 3. BBS1 is required for sustained signaling at the IS. (A,B) Immunofluorescence (IF) analysis of tyrosine phosphoproteins (p-Tyr) in conjugates of control (ctr) and BBS1 KD (J KD) Jurkat cells (A), or control (ctr) and BBS1 KO (T KO) primary T cells (B), with SEE- and SAg-loaded Raji cells (APCs), respectively. Representative images (medial optical sections) of the conjugates formed in the presence of SEE or SAgs are shown (see Fig. S4A,D for SEE- and SAg-independent conjugates). Graphs: Quantification (percentage) of 5 min and 15 min antigen-specific conjugates harboring p-Tyr staining at the IS (≥25 cells/sample, *n*=3, unpaired two-tailed Student's *t*-test) (left). Relative p-Tyr fluorescence intensity at the IS in 15 min conjugates of control (ctr) and BBS1 KD (J KD) Jurkat cells (A), or control (ctr) and BBS1 KO (T KO) primary T cells (B), with Raji cells in the absence or presence of SEE or SAgs (≥10 cells/sample, *n*=3, Kruskal–Wallis test) (right). (C,D) Immunofluorescence (IF) analysis of p-ZAP-70 (C) or p-LAT (D) in conjugates of control (ctr) and BBS1 KD (J KD) Jurkat cells with SEE-loaded Raji cells (APCs). Representative images (medial optical sections) of the conjugates formed in the presence of SEE are shown (see Fig. S4E,F for SEE-independent conjugates). Graphs: Quantification (percentage) of 5 min and 15 min SEE-specific conjugates harboring p-ZAP-70 (C) or p-LAT (D) at the IS (≥25 cells/sample, *n*=3, unpaired two-tailed Student's *t*-test) (left). Relative p-ZAP-70 (C) or p-LAT (D) fluorescence intensity at the IS in 15-min conjugates of control (ctr) and BBS1 KD (J KD) Jurkat cells with Raji cells in the absence or presence of SEE (≥15 cells/sample, *n*=3, Kruskal–Wallis test) (right). (E) Time-course flow cytometric analysis of protein tyrosine phosphorylation in conjugates of control (ctr) and BBS1 KO (J KO) Jurkat cells with SEE-loaded Raji cells (APCs). Raji cells were labeled with DiO and the analysis was carried out gating on DiO-negative (DiO^-) cells. Mean fluorescence intensities (MFIs) of $p\text{-}Tyr^+$ and DiO^- cells at different time points (*n*≥3, Mann–Whitney test) are shown. (F) Quantification (percentage) of 15 min SEE-specific conjugates of control (ctr) or BBS1 KO (J KO) Jurkat cells showing PCNT, CD3ζ and p-Tyr staining at the IS (≥25 cells/sample, *n*=3, unpaired two-tailed Student's *t*-test). Both ctr and J KO were transfected with the empty vector (ctr+GFP, J KO+GFP), and J KO were also transfected with the same vector encoding wild-type BBS1 (J KO+BBS1–GFP). Scale bars: 5 µm. Data are expressed as mean±s.d. ****$P\leq0.0001$; ***$P\leq0.001$; **$P\leq0.01$; *$P\leq0.05$; n.s., not significant.

investigated the impact of proteasome inhibition on the ability of T cells to form functional ISs. Two pharmacological proteasome inhibitors were used, MG132 and epoxomicin, to rule out off-target effects. Jurkat or primary T cells were pre-treated for 2 h with MG132 or epoxomicin and washed before conjugate formation. These pre-treatments resulted in the expected accumulation of ubiquitylated proteins, as assessed by immunoblot analysis of cell lysates (Fig. S7A), without any significant loss in cell viability (Fig. S7B) or CD3ε surface expression (Fig. S7C). Remarkably, proteasome inhibitor pre-treatment phenocopied the effects of BBS1 deficiency on IS assembly, with a defect in centrosome polarization, as assessed by co-staining conjugates with antibodies for centrosomal markers (Fig. 6A,D,E; Fig. S7D) and nesprin-2 (Fig. S7E). Additionally, the endosomal TCR–CD3 pool failed to translocate to the IS formed by treated cells (Fig. 6B,D,F; Fig. S7F), concomitant with impaired synaptic accumulation of TCR and tyrosine phosphoproteins (Fig. 6B–D,F,G; Fig. S7G,H), despite the ability of these cells to promote p-Tyr signaling at earlier stages of IS assembly (Fig. S7I). Similar to BBS1-deficient T cells, the centrosome-associated F-actin and WASH pools did not become depleted during IS formation in Jurkat (Fig. 6H,I) or primary (Fig. S7J) T cells pre-treated with proteasome inhibitors, while F-actin accumulation in the IS was unaffected (Fig. S7K). Although proteasome inhibition might result in alterations in other ubiquitin-regulated processes, these results suggest a functional link between the ubiquitin–proteasome system and the F-actin clearance-related centrosome translocation towards the T cell–APC interface, on which the assembly of a functional IS crucially depends.

The 19S regulatory subunit of the proteasome is recruited to the centrosome during IS assembly through BBS1-mediated coupling to dynein

The 26S proteasome consists of a 20S catalytic subunit and a 19S regulatory subunit (19S RP) that is essential not only for its proteolytic activity, but also for substrate recognition, unfolding and translocation into the 20S internal core (Bard et al., 2018). Although proteasome distribution is largely cytosolic, specific subcellular pools have been identified, of which one associates with the centrosome (Vora and Phillips, 2016). We hypothesized that, similar to B cells (Ibañez-Vega et al., 2019), the activity of the centrosome-associated proteasome in T cells could be regulated by the dynamic recruitment of its regulatory subunit during IS assembly to promote local F-actin clearance. To address this question, we imaged the 19S RP S4 [encoded by *PSMC1* (hereafter 19S RP)] associated with the centrosome at different time points after conjugate formation, using a 2 µm diameter mask to include solely the centrosome for the quantifications (Fig. S4C). A centrosomal accumulation of 19S RP was detected in control T cells under basal conditions, as assessed in conjugates formed in the absence of SEE and co-stained for γ-tubulin (Fig. 7A). This pool increased early during IS formation (1 min), before the stabilization of the IS to its mature architecture featuring centrosome polarization (15 min) (Fig. 7A). Interestingly, a lesser centrosomal 19S RP pool was observed under the same conditions in BBS1-deficient T cells compared to control cells (Fig. 7A,C; Fig. S5G). These results suggest that the activity of the centrosome-associated proteasome is upregulated during IS formation through 19S RP recruitment and that this process is regulated by BBS1. In agreement with this hypothesis, co-staining SEE-specific conjugates with anti-pan-ubiquitin and anti-PCNT antibodies revealed a centrosomal accumulation of ubiquitylated proteins in BBS1-deficient T cells (Fig. 7B). Similar results were obtained using an antibody that specifically recognizes proteins modified with K48-linked ubiquitin chains, which are targets of the proteasome (Walczak et al., 2012) (Fig. 7D; Fig. S8A), confirming that the accumulation of ubiquitylated proteins at the centrosome of BBS1 KD cells was related at least in part to defective proteasome activity. Consistent with the notion that the centrosomal pool is specifically affected by BBS1 deficiency, we did not observe a generalized defect in proteasome activity, as assessed by probing post-nuclear supernatants with an anti-pan-ubiquitin antibody (Fig. S7L). Of note, BBS1-deficient cells displayed a lesser centrosomal 19S RP pool compared to control cells also in the absence of activation (Fig. 7A,C), which was paralleled by a basal accumulation of ubiquitylated proteins (Fig. 7B,D), suggesting that BBS1 participates in the maintenance of the centrosome-associated proteasome.

Microtubule-dependent retrograde transport, involving coupling to the minus-end microtubule motor dynein, has been implicated in the regulation of local proteasome pools during axon development (Hsu et al., 2015). A similar process might account for the centrosomal accumulation of 19S RP. To address this issue, we assessed the ability of BBS1 to interact with 19S RP in co-immunoprecipitation assays on a Jurkat transfectant generated using GFP-tagged BBS1. BBS1 was found to associate constitutively with 19S RP (Fig. 7E). Consistent with the role of the BBSome in mediating cargo–dynein interactions during retrograde transport (Nakayama and Katoh, 2018), cytoplasmic dynein 1 intermediate chain 1 [endoded by *DYNC1I1* (hereafter dynein)] was also found to co-immunoprecipitate with BBS1–GFP (Fig. 7E). BBS1 deficiency led to a disruption of the interaction between 19S RP and dynein (Fig. 7F). Moreover, pre-treatment of control T cells with the dynein inhibitor ciliobrevin D led to a defect in 19S RP recruitment to the

Journal of Cell Science (2021) 134, jcs258462. doi:10.1242/jcs.258462

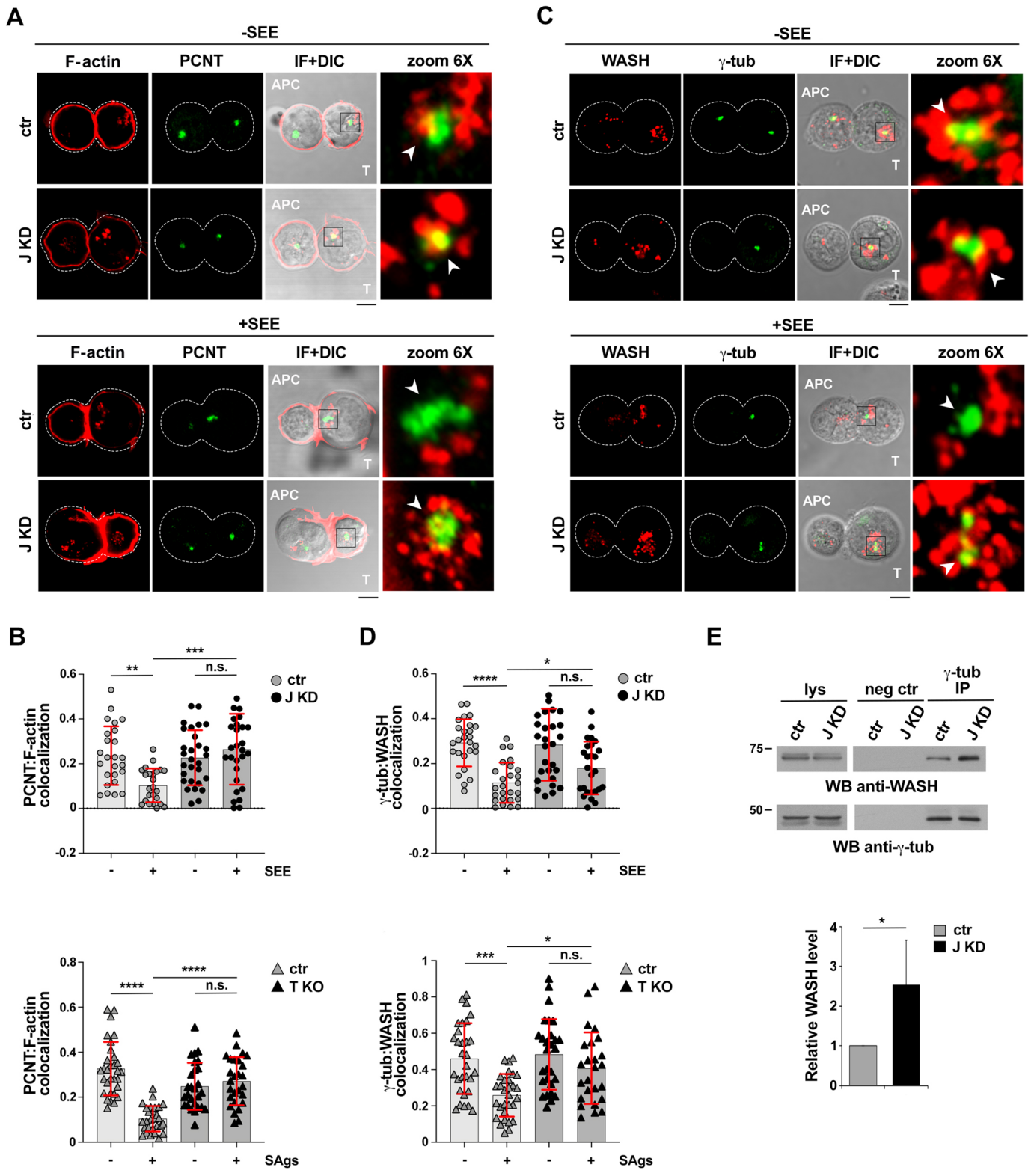

Fig. 4. See next page for legend.

centrosome (Fig. 7G; Fig. S8B), concomitant with a failure of the centrosome to polarize to the IS (legend to Fig. S8B), confirming the role of dynein in centrosome polarization in T cells (Martín-Cófreces et al., 2008) and providing evidence that dynein plays a key role in the transport of 19S RP to the centrosome during IS assembly.

Taken together, these results suggest that BBS1 promotes centrosome repositioning during IS assembly by assisting the dynein-dependent recruitment of 19S RP to the centrosome to allow for the proteasome-regulated clearance of centrosome-associated F-actin.

DISCUSSION

Based on rapidly accumulating evidence that proteins implicated in the growth and function of the primary cilium are co-opted by non-

Journal of Cell Science (2021) 134, jcs258462. doi:10.1242/jcs.258462

Fig. 4. BBS1 is required for centrosomal F-actin clearance during IS formation. (A) Immunofluorescence (IF) analysis of centrosomal F-actin (phalloidin) in 15 min conjugates of control (ctr) and BBS1 KD (J KD) Jurkat cells with Raji cells (APCs) in the absence or presence of SEE. Conjugates were co-stained for pericentrin (PCNT). Representative images (medial optical sections) are shown. Dashed lines mark the cell outlines. Boxes indicate regions shown in 6× zoom images, and arrowheads indicate the centrosomes. DIC, differential interference contrast. (B) Quantification using Manders' coefficient of the weighted colocalization of PCNT with centrosomal F-actin (see Fig. S4C for mask generation) in 15 min conjugates of control (ctr) and BBS1 KD (J KD) Jurkat cells (top), or control (ctr) and BBS1 KO (T KO) primary T cells (bottom), with Raji cells in the absence or presence of SEE or SAgs, respectively (≥10 cells/sample, n=3, Kruskal–Wallis test). (C) Immunofluorescence analysis of centrosomal WASH in 15 min conjugates of control (ctr) and BBS1 KD (J KD) Jurkat cells with Raji cells (APCs) in the absence or presence of SEE. Conjugates were co-stained for γ-tubulin (γ-tub). Representative images (medial optical sections) are shown. Dashed lines mark the cell outlines. Boxes indicate regions shown in 6× zoom images, and arrowheads indicate the centrosomes. (D) Quantification using Manders' coefficient of the weighted colocalization of γ-tubulin with centrosomal WASH (see Fig. S4C for mask generation) in 15 min conjugates of control (ctr) and BBS1 KD (J KD) Jurkat cells (top), or control (ctr) and BBS1 KO (T KO) primary T cells (bottom), with Raji cells in the absence or presence of SEE or Sags, respectively (≥10 cells/sample, n=3, Kruskal–Wallis test). (E) Top: Western blot (WB) analysis of γ-tubulin-specific immunoprecipitates from lysates of control (ctr) and BBS1 KD (J KD) Jurkat cells. A preclearing control (proteins that bound to Protein-A–Sepharose before addition of primary antibody) is shown (neg ctr). Total cell lysates (lys) were included in each gel to identify the migration of the tested proteins (≤1% of the total lysate). The migration of molecular mass markers is shown (kDa). Bottom: Bar graph showing the relative intensities of the immunoreactive bands corresponding to WASH (J KD versus ctr) normalized to the immunoprecipitated γ-tubulin (n=3, ctr value=1, one-sample t-test). Scale bars: 5 µm. Data are expressed as mean±s.d. ****P≤0.0001; ***P≤0.001; **P≤0.01; *P≤0.05; n.s., not significant.

ciliated cells to regulate basic processes, vesicular trafficking being a prominent example thereof (Onnis and Baldari, 2019), here we have explored the role of the BBSome component BBS1 in the formation of the T cell IS. We showed that BBS1 participates in IS assembly by promoting centrosome polarization towards the APC through clearance of centrosome-associated F-actin and its regulator WASH. The observation that proteasome inhibitors phenocopy the defects caused by BBS1 deficiency suggested a link between centrosome mobilization to the IS and activity of the centrosome-associated proteasome, involving BBS1. Consistent with this notion, we found that BBS1 couples the 19S regulatory subunit of the proteasome to dynein for its transport to the centrosome during the early stages of IS formation (Fig. 8). These results identify BBS1 as a key player in IS assembly.

BBS1 is responsible for binding BBS3 (Arl6) to promote BBSome entry into cilia (Mourão et al., 2014). Additionally, pre-BBSome assembly is primed by BBS4 at pericentriolar satellites, with basal body-resident BBS1 targeting the pre-BBSome to the base of the cilium to complete BBSome maturation locally (Prasai et al., 2020). Given this pivotal role of BBS1 in BBSome assembly, we believe that our results obtained on BBS1 could reflect the function of the entire BBS complex, as shown in ciliated cells (Liu et al., 2014; Starks et al., 2015; Guo et al., 2016). This notion is supported by the finding that BBS4 also polarizes to the IS together with the centrosome. However, we cannot rule out a BBSome-independent function of BBS1 in centrosome repositioning to the IS.

The role of the BBSome in ciliary protein trafficking has been extensively documented. Although its implication in protein entry into the cilium is still debated, the main function of the BBSome is to cooperate with the IFT-B complex in retrograde trafficking of ciliary receptors to the base of the cilium and their crossing of the transition zone before returning to the cell body (Nachury, 2018; Nakayama and Katoh, 2018). This trafficking-related function of the BBSome, which might result from its ability to polymerize a flat coat on synthetic membranes (Jin et al., 2010), has been reported for a number of receptors, GPCRs being the main group (Nozaki et al., 2018; Ye et al., 2018). Our results highlight an apparent divergence in the function of the BBSome in ciliated cells and in the non-ciliated T cells, since in the latter BBS1 is required for the transport of a cytosolic protein complex, the 19S proteasome subunit. However, since centrosome translocation is a prerequisite for reorientation of the secretory apparatus towards the IS and focalized exocytosis (Stinchcombe and Griffiths, 2014; Bustos-Morán et al., 2016), we cannot exclude that the BBSome is also implicated in trafficking events downstream of centrosome translocation during IS formation, in particular TCR recycling, in which IFT20 and other IFT-B complex components participate (Finetti et al., 2009, 2014).

The centrosome has been shown to promote the local polymerization of actin filaments through recruitment of Arp2/3 and its activator WASH (Farina et al., 2016). A central function of this F-actin is to anchor the centrosome to the nucleus via interaction with the LINC complex (Burakov and Nadezhdina, 2013). During IS assembly, the centrosome-associated F-actin pool undergoes depletion (Bustos-Morán et al., 2016; Bello-Gamboa et al., 2020). In B cells, this has been demonstrated to be caused by a relocalization of Arp2/3 from the centrosome to the IS, which leads to centrosome detachment from the nucleus, allowing for its polarization (Obino et al., 2016). Here, we show that centrosome-associated F-actin clearance is impaired in BBS1-deficient T cells undergoing IS assembly concomitant with the persistence of a centrosomal pool of WASH, which might account for the failure of the centrosome to dissociate from the nuclear membrane and translocate towards the T cell–APC contact. The defect in centrosome translocation would in turn prevent polarization of endosomal TCRs towards the IS, which is a prerequisite for their delivery to the synaptic membrane (Soares et al., 2013; Bustos-Morán et al., 2016). Of note, dissociation from the nucleus is not required for centrosome polarization to the IS formed by CTLs (Lui-Roberts et al., 2012). Our results, obtained on a $CD4^+$ T cell-derived line and on primary peripheral T cells, and confirmed on purified $CD4^+$ T cells, suggest that T cells other than CTLs might be more dependent on centrosome dissociation from the nucleus for its synaptic repositioning. Interestingly, recycling TCRs fail to polarize towards the IS also in T cells deficient for other ciliogenesis proteins, despite a normal repositioning of the centrosome (Finetti et al., 2009, 2014; Onnis et al., 2015; Capitani et al., 2021) resulting from their role in other steps of the pathway, such as sorting at early endosomes or coupling to microtubule motors, underscoring non-redundant roles of these proteins in IS assembly.

Interestingly, a proteomic analysis of centrosomes purified from activated T cells has recently provided evidence of a local activation-dependent accumulation of proteins implicated in protein folding and degradation, including the proteasome (Martin-Cofreces et al., 2020). Taken together with the proteasome accumulation at the centrosome during B cell IS assembly (Ibañez-Vega et al., 2019), these reports highlight the centrosome as a control center for protein degradation in lymphocytes. Our findings provide a link between proteasome accumulation at the centrosome and centrosomal F-actin clearance. Although we cannot rule out effects of the proteasome inhibitors used in this study on other processes upstream of centrosomal F-actin clearance, the fact that surface TCR levels and early p-Tyr signaling were not affected by the 2 h pre-treatment support the implication of the proteasome in centrosomal F-actin clearance during IS assembly. The molecular targets of the centrosome-associated proteasome that

Journal of Cell Science (2021) 134, jcs258462. doi:10.1242/jcs.258462

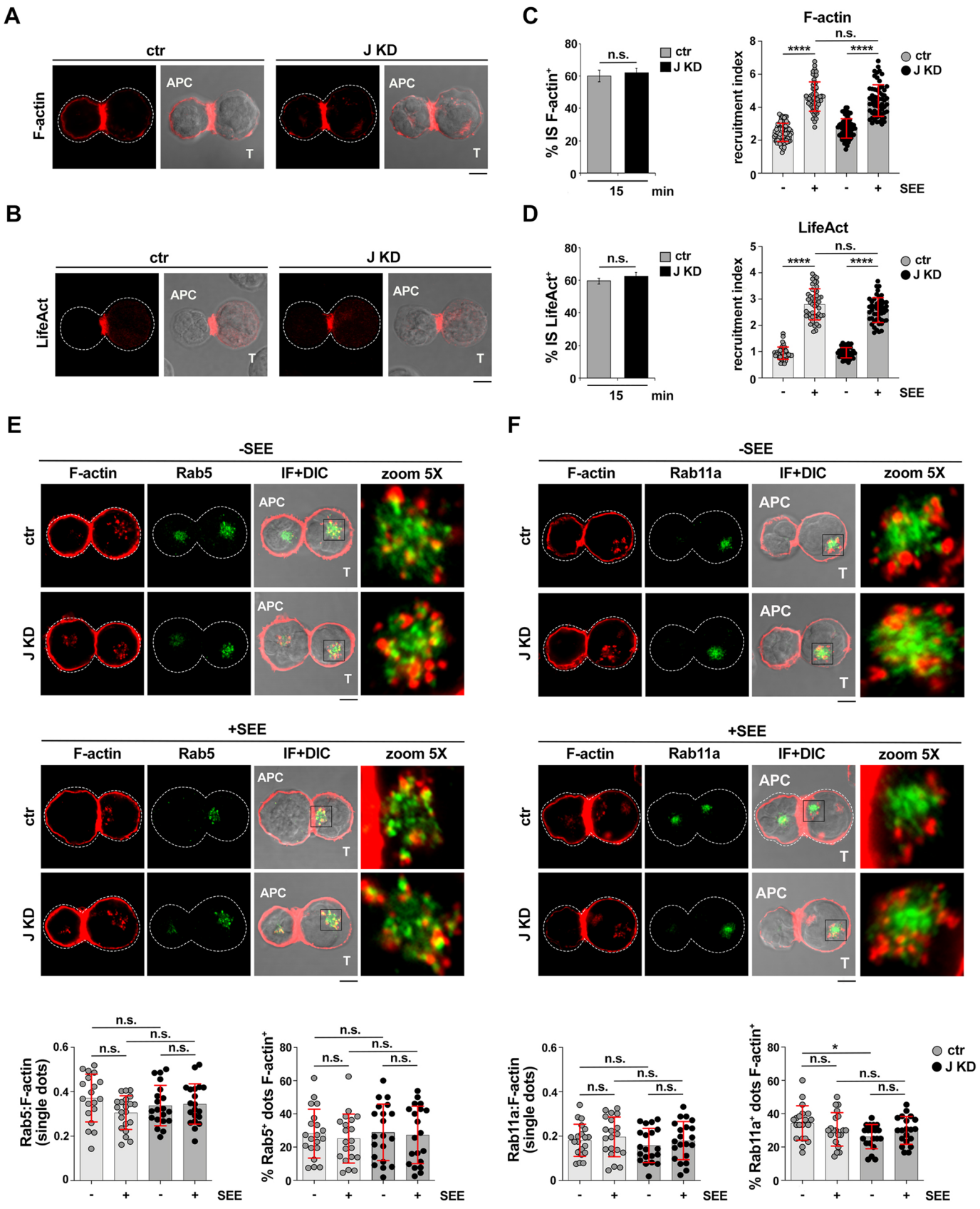

Fig. 5. See next page for legend.

Journal of Cell Science

Fig. 5. BBS1 is dispensable for synaptic F-actin accumulation and endosomal F-actin dynamics. (A,B) Immunofluorescence (IF) analysis of F-actin in control and BBS1 KD (J KD) Jurkat cells (A), or control and BBS1 KD (J KD) Jurkat cells transiently transfected with the LifeAct reporter (B), and conjugated with SEE-loaded or with unloaded Raji cells (APCs) for 15 min. Representative images (medial optical sections) of the conjugates formed in the presence of SEE are shown (see Fig. S4G,H for SEE-independent conjugates). DIC, differential interference contrast. (C,D) Left: Quantification (percentage) of 15 min SEE-specific conjugates harboring F-actin (C) and LifeAct (D) staining at the IS (≥25 cells/sample, n≥3, unpaired two-tailed Student's t-test). Right: Relative F-actin (C) or LifeAct (D) fluorescence intensity at the IS in 15 min conjugates of control (ctr) and BBS1 KD (J KD) Jurkat cells with Raji cells in the absence or presence of SEE (≥15 cells/sample, n=3, Kruskal–Wallis test). (E,F) Top: Immunofluorescence (IF) analysis of endosomal F-actin in 15 min conjugates of control (ctr) and BBS1 KD (J KD) Jurkat cells with Raji cells (APCs) in the absence or presence of SEE. Conjugates were co-stained for Rab5 (E) and Rab11a (F) (see Fig. S4C for mask generation). Boxes indicate regions shown in 5× zoom images. DIC, differential interference contrast. Bottom: Colocalization of F-actin on individual dots (left) and quantification of Rab5$^+$ (E) or Rab11a$^+$ (F) dots positive for F-actin (right) (10 cells/sample, 15 dots/cell, n=2, Kruskal–Wallis test or one-way ANOVA based on normality distribution of different data sets). Scale bars: 5 µm. Dashed lines in A,B,E,F indicate cell outlines. The data are expressed as mean±s.d. ****P≤0.0001; *P≤0.05; n.s., not significant.

undergo degradation to allow for local F-actin clearance remain to be elucidated. Our finding that the centrosome-associated WASH pool becomes depleted during IS formation highlights WASH as a possible candidate. Although to date there is no published evidence of a proteasomal regulation of WASH itself, the activity of WASH is indirectly regulated by the proteasome, which degrades the E3 ubiquitin ligase TRIM27 that activates WASH by non-degradative K63-linked ubiquitylation (Hao et al., 2013). Additionally, several proteins that promote F-actin nucleation by binding the Arp2/3 complex are regulated by proteasome-mediated degradation, including WASp (Watanabe et al., 2013) and WAVE2 (also known as WASF2) (Joseph et al., 2017). Another potential proteasome-regulated target is the centriolar satellite protein PCM1 (Didier et al., 2008), which contributes to the actin-nucleating function of the centrosome by recruiting WASH and Arp2/3 (Farina et al., 2016). Degradation of any of these proteins by the centrosome-associated proteasome is expected to slow down the rate of F-actin polymerization, leading to a shift of actin dynamics towards turnover.

Our findings identify BBS1 as a new player in the process that regulates proteasome accumulation at the centrosome. The impairment in 19S RP recruitment to the centrosome of BBS1-deficient T cells at early stages of IS assembly, when the centrosome undergoes polarization to the nascent IS, paralleled by an accumulation of ubiquitylated proteins around the centrosome, supports the notion that BBS1 modulates the centrosome-associated proteasome. To carry out this function, it exploits its documented cilia-related retrograde trafficking function to couple 19S RP to dynein. This observation could account, at least in part, for the defects in centrosome polarization to the IS observed in T cells with defective activity of the dynein–dynactin or dynein–NDE1 complexes (Martíin-Cófreces et al., 2008; Nath et al., 2016). It is noteworthy that BBS proteins have been shown to interact with proteasome subunits in ciliated cells, and that their loss leads to proteasome depletion from the centrosome (Liu et al., 2014). Although the underlying mechanism has not been investigated, these data suggest a conserved, cilia-independent function of BBS proteins in centrosome proteostasis in ciliated and non-ciliated cells. Interestingly, the BBSome also interacts with ubiquitin to promote the removal of smoothened (SMO) and other GPCRs from the ciliary membrane (Xu et al., 2015; Langousis et al., 2016; Desai et al., 2020). This function might be relevant for the fate of post-endocytic synaptic TCRs.

BBS is a pleiotropic genetic disorder characterized by a number of abnormalities that include polydactyly, kidney dysfunction, obesity, hypogonadism and anosmia (Forsythe and Beales, 2013; Tsang et al., 2018). These defects are caused by dysfunction of primary cilia, which in general grow normally but are unable to signal because of impaired BBSome-mediated ciliary trafficking of components of signaling pathways, such as the sonic hedgehog (Shh) pathway (Mourão et al., 2016). The potential impact of BBS-related mutations on the immune system had not been addressed until recently. We have recently reported immune abnormalities in BBS patients, which are associated with a higher incidence of autoimmune diseases (Tsyklauri et al., 2021). Using the *Bbs4*$^{-/-}$ mouse model of BBS, we showed that BBS4 deficiency affects mainly the B-cell compartment through a non-intrinsic mechanism that remains to be defined, with only minor effects on the T cell compartment. However, we did not observe any significant effect of BBS4 deficiency on mouse B cell and T cell responses (Tsyklauri et al., 2021). The results presented in this report, implicating BBS1 in IS assembly, are in apparent contrast with these findings. We can propose several factors that could underlie these differences. First, here we have used human T cells, and emerging evidence has highlighted features of the human immune response that are not recapitulated in the mouse system (Mestas and Hughes, 2004; Bjornson-Hooper et al., 2019 preprint). Second, BBS1 and BBS4 carry out complementary yet different functions in BBSome assembly (Prasai et al., 2020). Additionally, despite the fact that both BBS1 and BBS4 co-polarize to the IS, we cannot rule out at this stage BBSome-independent functions of BBS1 and BBS4 in T cells or other non-ciliated cells. Third, the fact that no defects in conjugate formation have been observed in mouse *Bbs4*$^{-/-}$ T cells (Tsyklauri et al., 2021) suggests that T cell adhesion to APCs is normal, but does not exclude defects in IS assembly. Finally, compensatory mechanisms may account for the normal *in vivo* *Bbs4*$^{-/-}$ T cell response in the diabetes mouse model used in our previous report (Tsyklauri et al., 2021).

The study of T cells from BBS patients will shed light on the outcome of BBSome dysfunction on T cell IS formation and on the downstream events. Nonetheless, the fact that all BBSome components are expressed in T cells, the immune defects observed in BBS patients (Tsyklauri et al., 2021) and the data presented in this report open a new perspective in the search for gene defects in primary immunodeficiencies of unknown etiology.

MATERIALS AND METHODS

Cells, plasmids and antibodies

Cells included Jurkat T cells, Raji and Ramos B cells, and BJ-5ta fibroblasts (ATCC, Manassas, VA). Cells were periodically treated with Plasmocure™ (Invivogen, San Diego, CA, #ant-pc) to prevent mycoplasma contamination. Buffy coats from anonymous healthy donors obtained from the Siena University Hospital blood bank were used for this study. The study was approved by the local ethics committee (Siena University Hospital). Informed consent was obtained from blood donors by the physician in charge of the Siena University Hospital blood bank. Samples were anonymized before distribution. Primary total and CD4$^+$ T cells were isolated from peripheral blood of healthy donors by negative selection using RosetteSep™ Human T Cell Enrichment Cocktail (STEMCELL Technologies, #5061) and RosetteSep™ Human CD4$^+$ T Cell Enrichment Cocktail (STEMCELL Technologies, #15062), respectively, and activated with Dynabeads® Human T-Activator CD3/CD28 (Thermo Fisher Scientific, #111.13D) for 48 h. B and T lymphocyte cell lines as well as primary T cells were grown at 37°C, 5% CO_2, in RPMI-1640 medium (Merck, #R8758) supplemented with 10% iron-

Journal of Cell Science (2021) 134, jcs258462. doi:10.1242/jcs.258462

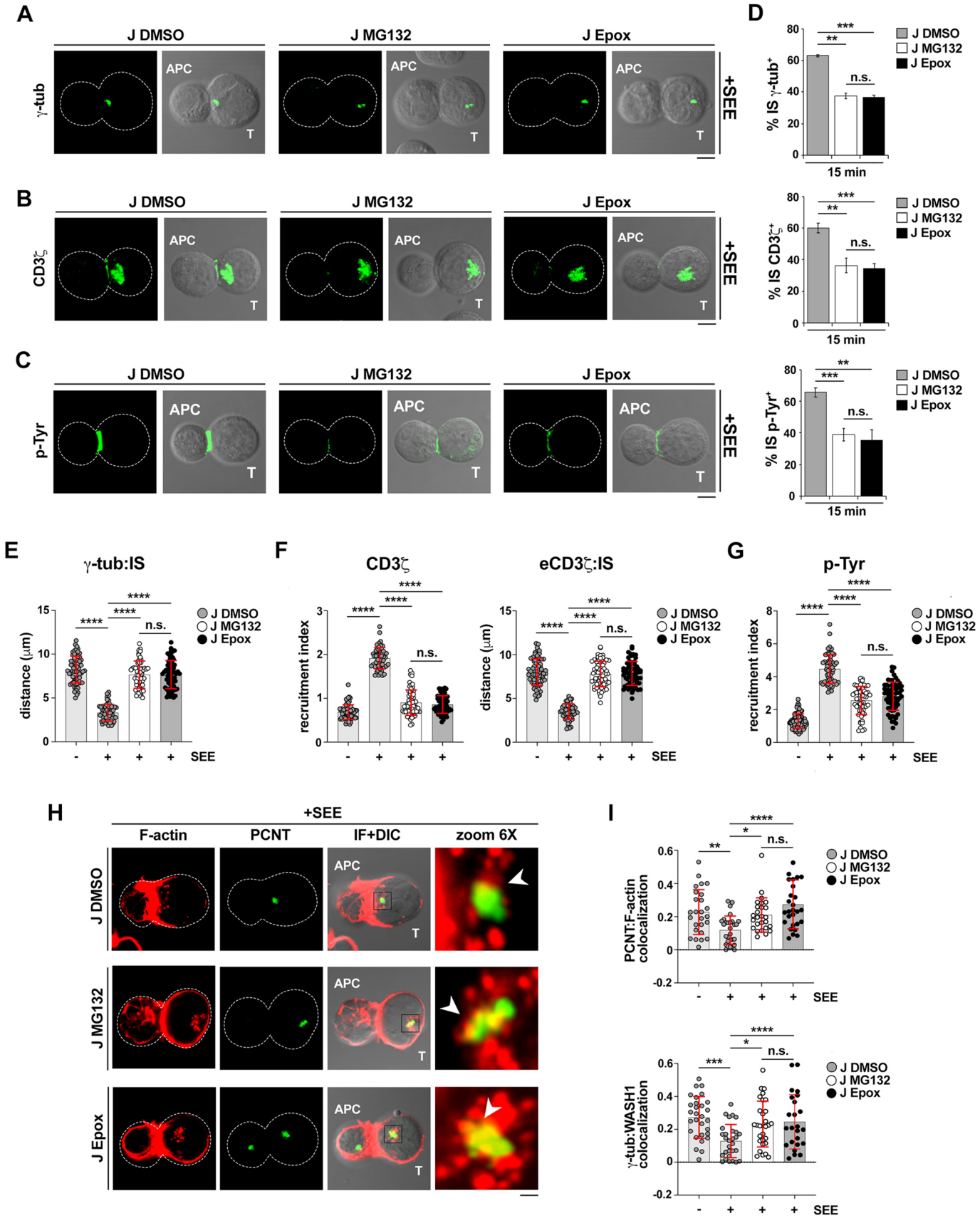

Fig. 6. See next page for legend.

Journal of Cell Science

Fig. 6. Centrosome translocation to the IS is regulated by the proteasome. (A,B,C,H) Immunofluorescence (IF) analysis of centrosome (γ-tubulin; γ-tub) (A), CD3ζ (B), tyrosine phosphoproteins (p-Tyr) (C) and centrosomal F-actin (H) in control Jurkat cells, pre-treated with either carrier (DMSO) or the proteasome inhibitors MG132 or epoxomicin (Epox), and conjugated with Raji cells (APCs) in the absence or presence of SEE for 15 min. Representative images (medial optical sections) of the conjugates formed in the presence of SEE are shown. Dashed lines indicate cell outlines. Boxes mark regions shown in 6× zoom images and arrowheads indicate the centrosomes. DIC, differential interference contrast. (D) Quantification (percentage) of 15 min SEE-specific conjugates formed by control Jurkat cells pre-treated with carrier (J DMSO), MG132 (J MG132) or epoxomicin (J Epox) and harboring γ-tubulin (top), CD3ζ (middle) or p-Tyr (bottom) staining at the IS (≥25 cells/sample, *n*=3, unpaired two-tailed Student's *t*-test). (E–G) Measurement of the distance (μm) of the centrosome (γ-tubulin) from the T cell–APC contact site (E), relative CD3ζ fluorescence intensity at the IS (F, left), measurement of the distance (μm) of the endosomal TCR–CD3 pool (eCD3ζ) from the T cell–APC contact site (F, right) and relative p-Tyr fluorescence intensity at the IS (G) in control (ctr) Jurkat cells, pre-treated with either carrier (DMSO) or the proteasome inhibitors MG132 or epoxomicin, and conjugated with Raji cells (APCs) in the absence or presence of SEE for 15 min (≥10 cells/sample, *n*=3, Kruskal–Wallis test). (I) Quantification using Manders' coefficient of the weighted colocalization of PCNT with centrosomal F-actin (top) or γ-tubulin with centrosomal WASH (bottom) in control Jurkat cells, pre-treated with carrier (DMSO), or with the proteasome inhibitors MG132 or epoxomicin (see Fig. S4C for mask generation), and conjugated with Raji cells (APCs) in the absence or presence of SEE for 15 min (≥10 cells/sample, *n*=3, Kruskal–Wallis test). Scale bars: 5 μm. Data are expressed as mean±s.d. ****$P \leq 0.0001$; ***$P \leq 0.001$; **$P \leq 0.01$; *$P \leq 0.05$; n.s., not significant.

enriched bovine calf serum (BCS; HyClone, GE Healthcare, #SH30072.03) and 50 U/ml of human IL-2 Improved Sequence (Miltenyi Biotec, #130-097-142) for primary T cells. BJ-5ta fibroblasts were kept in a 4:1 mixture of Dulbecco's medium (Merck, #D6429) and Medium 199 (Gibco, #31153) supplemented with 10% fetal bovine serum (FBS; Euroclone, #ECS0180 L) and 0.01 mg/ml hygromycin B (Invitrogen, #10687010).

Plasmids included Mission® pLKO-puro Non-Target shRNA (Merck, #SHC016V), pLKO shRNA targeting BBS1 (Merck, #TRCN0000417688), and pEGFP-N1-BBS1. Since the anti-BBS1 antibodies tested gave a strong background noise that prevented their use, we generated a construct encoding a C-terminal GFP-tagged BBS1 (BBS1–GFP) by amplifying the full-length CDS sequence of BBS1 from pCS2-Myc6-BBS1 vector (Jin et al., 2010) and by subcloning the PCR product into the pEGFP-N1 backbone (Follit et al., 2006) using *Eco*RI and *Bam*HI restrictions sites. Both transient and stable BBS1–GFP-expressing transfectants showed some cytoplasmic staining, which could result from partial cleavage of BBS1–GFP leading to freely diffusible GFP, as confirmed by immunoblotting (data not shown), even though we cannot rule out the existence of a cytosolic BBS1 pool. To construct an N-terminal SYFP-tagged BBS4 (SYFP–BBS4), the BBS4 open reading frame was amplified from cDNA obtained from hTERT-RPE-1 (ATCC, Manassas, VA) cells and the SYFP coding region was added at the 5′ end using recombinant PCR, and cloned into pMSCV retroviral vector using *Eco*RI and *Cla*I restriction sites (Prasai et al., 2020). A construct encoding the F-actin reporter mApple–LifeAct-7 was purchased from Addgene (#54747; deposited by Davidson's laboratory).

All primary commercial antibodies used in this work are listed in Table S2, together with information about the dilutions used for immunoblotting, immunofluorescence, immunoprecipitation and flow cytometry. Secondary horseradish peroxidase (HRP)-labeled antibodies were purchased from Jackson ImmunoResearch Laboratories (anti-mouse, #115-035-146; anti-rabbit, #111-035-14), and Alexa Fluor 488-, 555- and 647-labeled secondary antibodies were from ThermoFisher Scientific (anti-mouse 488, #A11001; anti-rabbit 488, #A11008; anti mouse 555, #A211422; anti-rabbit 555, #A21428; anti-mouse 647, #A21236; anti-mouse 647, #A21235).

Generation of stable Jurkat transfectants, transfection and transduction methods

A stable BBS1-depleted Jurkat T cell line was generated by transducing cells with commercial lentiviral particles carrying a non-targeting control shRNA (ctr) or an shRNA specific for BBS1 (J KD) and selecting in puromycin-containing medium at a final concentration of 3 μg/ml (Merck, #P8833). Knockdown Jurkat cells were routinely checked for BBS1 expression by immunoblotting. In order to generate a stable transfectant expressing BBS1–GFP, Jurkat cells were transfected by electroporation (Gene Pulser II, Bio-Rad) and monoclonal cell lines were selected in Geneticin Selective Antibiotic (G418 Sulfate; ThermoFisher Scientific, #11811-031)-containing medium at a final concentration of 2 mg/ml. Cell clones expressing BBS1–GFP at the highest levels were screened by flow cytometry and routinely checked by immunoblotting and immunofluorescence. Equal numbers of cells from the three highest expressing clones were pooled for experiments. Transient transfection of Jurkat cells with either the BBS1–GFP construct (DNA:cells ratio=1 μg:10^6 cells) or the mApple–Lifeact-7 construct (DNA:cells ratio=1.5 μg:10^6 cells) was carried out using a modification of the DEAE-dextran procedure as described previously (Baldari et al., 1992) and cells were conjugated with either loaded or unloaded Raji cells (APCs) 24 h after transfection. Pseudoviral particles encoding N-terminally tagged SYFP–BBS4 were produced by transfecting 30 μg of vector SYFP2–BBS4 pMSCV DNA (Prasai et al., 2020) into Phoenix-Ampho cells (ATCC, Manassas, VA) using 1 μg/μl polyethylenimine (Polysciences, #23966-2). Jurkat cells were transduced by incubation with 2 ml of the virus-containing supernatant supplemented with 12 μg/ml Polybrene (Merck, #TR-1003) and centrifuged (45 min, 800 ***g***, 30°C). Stable SYFP-expressing cells were sorted using a BD Influx Cell Sorter (BD Biosciences). Transient transfection of activated primary T cells with the BBS1–GFP construct (DNA:cells ratio=2 μg:10^6 cells) was carried out using the Human T cell Nucleofector Kit (Amaxa Biosystems, #VPA-1002) and the Amaxa Nucleofector II system (Lonza), Program T-023 and cells conjugated with SAg-loaded Raji cells (APCs) 24 h after transfection.

Gene editing of Jurkat cells and activated primary T cells using CRISPR-Cas9 technology

Specific single guide RNAs (gRNAs) directing the nuclease Cas9 to *BBS1* gene (Table S1) were designed using the web-based tool CRISPOR (Haeussler et al., 2016). For gene editing of Jurkat T cells, guide RNA (gRNA) sequences were cloned into pSpCas9(BB)-2A-GFP (PX458) plasmid (Addgene, #48138; deposited by F. Zhang) as described elsewhere (Ran et al., 2013) and Jurkat cells were transfected with either empty vector or the gRNA-encoding constructs using Nucleofector Solution 2 M (5 mM KCl, 15 mM $MgCl_2$, 15 mM HEPES, 150 mM Na_2HPO_4/NaH_2PO_4 pH 7.2, 50 mM mannitol) (Chicaybam et al., 2013) and the Amaxa Nucleofector II system (Lonza), Program X-005. GFP-expressing cells were sorted, subcloned, and screened by immunoblotting. For gene editing of primary T cells, a gRNA transcription template was prepared by PCR amplification using the PX458 construct as a template and the primers listed in Table S1, and then transcribed *in vitro* using a HiScribe™ T7 High Yield RNA Synthesis Kit (NEB, #E2040S). gRNA was purified by RNA Clean & Concentration™ (Zymos Research, #R1017). Freshly isolated T cells were activated by incubation with anti-CD3/CD28 Dynabeads for 48 h in complete RPMI-1640 medium. Activated cells were transfected using the Human T cell Nucleofector Kit and the Amaxa Nucleofector II system, Program T-023 with ribonucleoprotein complexes, which were formed by mixing 5 μg of Alt-R® S.p. Cas9 Nuclease V3 protein (Integrated DNA Technologies, #1081059) and 3 μg of gRNA. Cells were allowed to recover in complete RPMI-1640 medium supplemented with 500 U/ml of human IL-2 for 72 h and then tested for gene editing by immunoblotting.

Conjugate formation

In IS experiments, Raji B cells (used as APCs) were loaded with 10 μg/ml of staphylococcal enterotoxin A (SEA; Toxin Technologies, #AT101), staphylococcal enterotoxin B (SEB; Toxin Technologies, #BT202) and staphylococcal enterotoxin E (SEE; Toxin Technologies, #ET404) for 2 h and labelled with 10 μM Cell Tracker Blue for the last 20 min of the incubation with SAgs. In particular, SEE was used for Jurkat cells that express TCR Vβ8, whereas a combination of SEA, SEB and SEE was used for primary T cells to cover a substantial proportion of the TCR Vβ repertoire compared with SEE alone. Antigen-independent conjugates of T cells with unloaded Raji B cells were used as negative controls.

Journal of Cell Science (2021) 134, jcs258462. doi:10.1242/jcs.258462

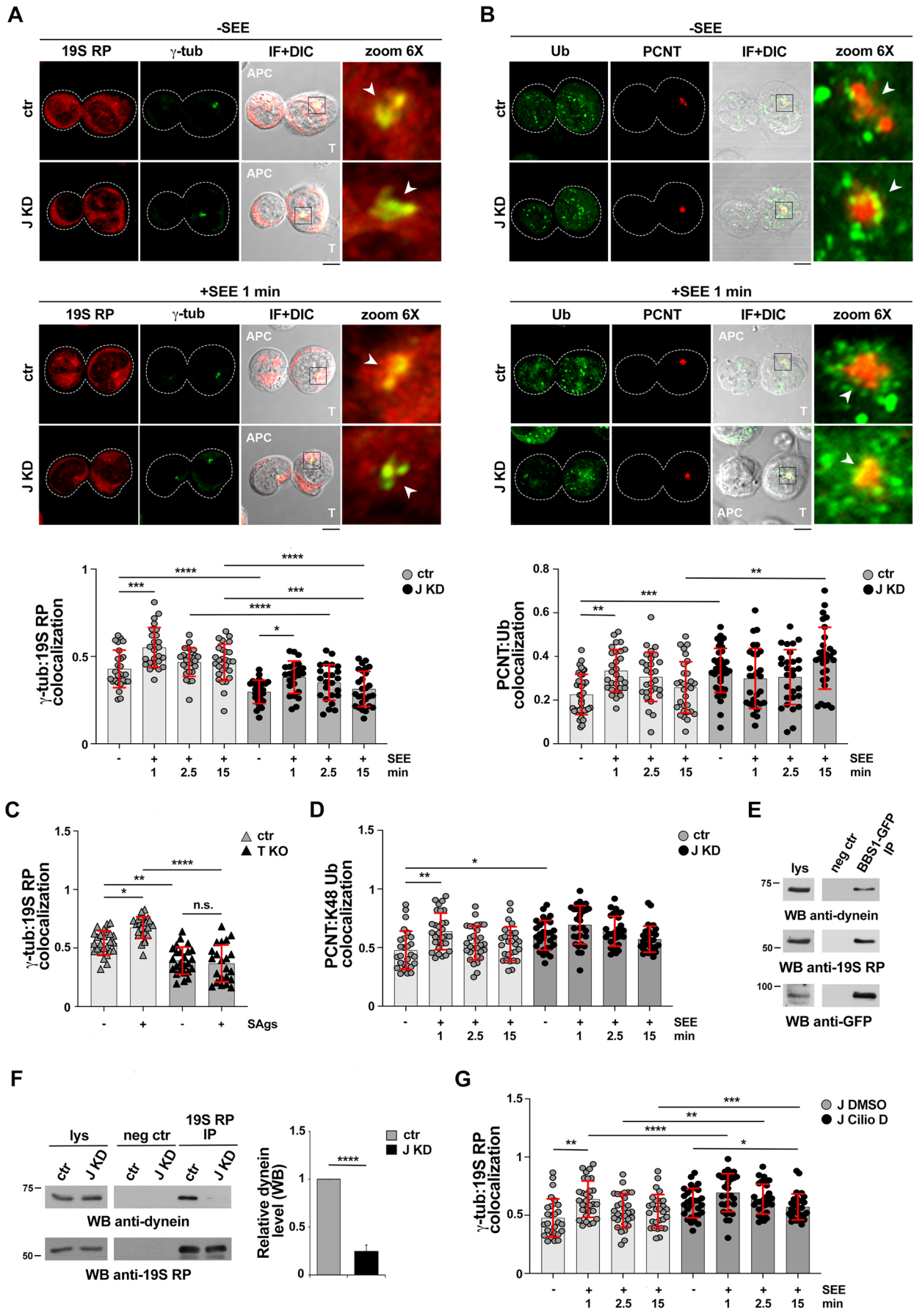

Fig. 7. See next page for legend.

Journal of Cell Science

Fig. 7. The 19S regulatory subunit of the proteasome is recruited to the centrosome during IS assembly through BBS1-mediated coupling to dynein. (A,B,D) Time-course immunofluorescence (IF) analysis of 19S RP recruitment (A), ubiquitylated proteins (Ub) (B) and K48-linked polyubiquitylated proteins (K48 Ub) (D) to the centrosome in conjugates of control (ctr) and BBS1 KD (J KD) Jurkat cells conjugated with SEE-loaded Raji cells (1, 2.5, 15 min) or with unloaded Raji cells (1 min) seeded on poly-L-lysine-coated slides. Conjugates were co-stained with γ-tubulin (γ-tub) (A) or pericentrin (PCNT) (B,D). Representative images (medial optical sections) of 1 min conjugates are shown for A and B. Dashed lines in A and B mark cell outlines, boxes highlight regions shown in 6× zoom images and arrowheads indicate the centrosomes. Quantification using Manders' coefficient of the weighted colocalization of 19S RP (A), Ub (B) and K48 Ub (D) with the centrosomal markers γ-tubulin (A) and PCNT (B,D) (see Fig. S4C for mask generation) (≥10 cells/sample, *n*=3, one-way ANOVA test or Kruskal–Wallis test based on normality distribution of different data sets). DIC, differential interference contrast. (C) Immunofluorescence analysis of 19S RP recruitment to the centrosome (γ-tubulin) in 1 min conjugates of control (ctr) and BBS1 KO (T KO) T cells added to Raji cells in the presence or absence of SAgs. Quantification using Manders' coefficient of the weighted colocalization of 19S RP with the centrosome (γ-tubulin) (≥10 cells/sample, *n*=3, Kruskal–Wallis test). (E,F) Western blot (WB) analysis of GFP-specific immunoprecipitates from lysates of BBS1–GFP-expressing cells (E). Western blot (WB) analysis of 19S RP-specific immunoprecipitates from lysates of control (ctr) and BBS1 KD (J KD) Jurkat cells (F). A preclearing control (proteins that bound to Protein-A–Sepharose before addition of primary antibody) is shown (E,F neg ctr). Total cell lysates (lys) were included in each gel to identify the migration of the tested proteins (≤1% of total lysate). The migration of molecular mass markers is shown (kDa). The bar graph in F shows the relative intensities of the immunoreactive bands corresponding to dynein (anti-cytoplasmic dynein 1 intermediate chain 1 antibody, clone 74.1; J KD versus ctr) normalized to immunoprecipitated 19S RP (mean±s.d., *n*≥3, ctr value=1, one-sample *t*-test). (G) Time-course immunofluorescence (IF) analysis of 19S RP recruitment to the centrosome (γ-tubulin) in conjugates of control Jurkat cells treated either with carrier (J DMSO) or 50 µM ciliobrevin D (J Cilio D) during conjugate formation with SEE-loaded Raji cells (1, 2.5, 15 min) or with unloaded Raji cells (1 min) seeded on poly-L-lysine-coated slides. Quantification using Manders' coefficient of the weighted colocalization of 19S RP with the centrosome (γ-tubulin) (≥10 cells/sample, *n*=3, Kruskal–Wallis test). Scale bars: 5 µm. Data are expressed as mean±s.d. Only statistically significant differences are shown. ****$P \leq 0.0001$; ***$P \leq 0.001$; **$P \leq 0.01$; *$P \leq 0.05$.

SEE- and SAg-loaded or unloaded Raji B cells were washed twice and mixed with Jurkat cells or primary T cells (1:1), and conjugates were analyzed at the indicated time points after conjugate formation (i.e. 5 and 15 min). Samples were seeded on to poly-L-lysine (Merck, #P1274)-coated slides (ThermoFisher Scientific, #X2XER208B) and fixed for 10 min in methanol at −20°C or for 15 min with 4% paraformaldehyde/PBS at room temperature. To image 19S RP at earlier points after conjugate formation (i.e. 0, 1, 2.5 and 15 min) we used a two-step protocol, with Raji B cells first seeded on poly-L-lysine-coated slides and allowed to adhere for 15 min at 37°C, followed by the addition of T cells and incubation at 37°C for the indicated time points before fixation.

To analyze SYFP–BBS4 localization (Fig. S1B), Ramos B cells, used as APCs, were loaded with 1 µM SEE (Toxin Technologies, #ET404) for 45 min and labelled with 1 µM CellTrace Violet stain (Thermo Fisher Scientific, #C34557). SEE-loaded Ramos B cells were washed twice, mixed with SYFP–BBS4-expressing Jurkat T cells (1:1) and plated on poly-L-lysine (Merck, #P8920)-coated coverslips. Cells were spun down (2 min, 1000 ***g***, room temperature) and incubated for 30 min at 37°C. Samples were briefly fixed in 4% formaldehyde/PBS at room temperature for 5 min, then in methanol for 20 min on ice and stained with Tu-30 antibody against γ-tubulin (a kind gift from Dr Pavel Dráber, IMG, Prague).

To assess the role of the proteasome in IS formation, Jurkat or primary T cells were pre-treated for 2 h with two different proteasome inhibitors, MG132 (10 µM; Merck, #M7449) or epoxomicin (10 µM; Abcam, #ab144598), before conjugate formation. None of the treatments affected cell viability at the concentrations and times chosen for the analyses, as assessed by Trypan Blue (Merck, #T8154) exclusion (Fig. S7B). To inhibit dynein during IS assembly, Jurkat cells were resuspended in medium containing ciliobrevin D (50 µM; Merck, #250401) and mixed with SEE-Raji B cells for conjugate formation.

Immunofluorescence acquisition and analysis

Following fixation, samples were washed in PBS for 5 min and stained with primary antibodies overnight at 4°C. After washing with PBS, samples were incubated for 45 min at room temperature with Alexa Fluor 488- and 555-labeled secondary antibodies and mounted with 90% glycerol/PBS.

Confocal microscopy was carried out on a Zeiss LSM700 (Carl Zeiss, Jena, Germany) or a TCS SP8 (Leica Microsystems, Wetzlar, Germany) microscope using a 63×/1.40 oil immersion objective. Images were acquired with pinholes opened to obtain 0.8 µm-thick sections. Detectors were set to detect an optimal signal below the saturation limits. Images were processed with Zen 2009 image software (Carl Zeiss). To analyze SYFP–BBS4 localization (Fig. S1B), widefield imaging was performed on a DeltaVision image fluorescence microscope (Applied Precision/Olympus) equipped with a CoolSnap HQ camera (Photometrics). Samples were imaged using a 40×/1.35 UApo/340 oil immersion objective.

Colocalization analyses were carried out on medial optical sections of either single cells or T cell–APC conjugates using ImageJ (https://imagej.nih.gov/ij/) and the JACoP plugin to calculate Manders' coefficient M_1, which indicates the proportion of the green signal coincident with a signal in the red channel over its total intensity, and M_2, which is defined conversely for red (Manders et al., 1992). Manders' coefficients range from 0 to 1, corresponding to non-overlapping images and 100% colocalization between both images, respectively.

In conjugates of T cells with antigen-loaded versus unloaded Raji B cells, relative distances of the centrosome from either the contact site with the APC (Manders et al., 1992) or the nuclear membrane (Farina et al., 2016) were measured using ImageJ (Fig. S2). Scoring of conjugates for clustering of γ-tubulin, CD3ζ, p-Tyr, p-ZAP-70, p-LAT and F-actin at the IS was based on the presence of the respective staining solely at the T cell–APC contact site and was expressed as percentage of conjugates with synaptic staining versus the total number of conjugates analyzed. The recruitment index was calculated for each marker as the ratio of CD3ζ, p-Tyr and F-actin fluorescence intensity at the synaptic area, which is manually defined at the T cell–APC contact site, to the entire cell using ImageJ. Values above 1 indicate an accumulation of the marker at the IS area compared to the entire cell, whereas values below 1 indicate a depletion of the marker at the IS area compared to the entire cell. Colocalization analyses shown in Fig. 4B,D, Fig. 6I, Fig. 7A–D,G, Fig. S5F,G, Fig. S7J were carried out on confocal images by calculating Manders' coefficients M_1 and M_2 in a 2 µm (Jurkat cells) or 1.2 µm (primary T cells) diameter circle around the centrosome (Fig. S4C) (Farina et al., 2016). Colocalization analyses shown in Fig. 5E,F, Fig. S6C,D were carried out on an endosome-enriched area corresponding to a 4.5 µm-diameter circle around the centrosome (Fig. 4C). The colocalization analysis shown in Fig. S6B was carried out on an endosome-enriched ring corresponding to a 4.5 µm-diameter circle around the centrosome, from which a 2 µm diameter circle (centrosomal area) was excluded.

RNA purification and RT-qPCR

RNA was extracted from Jurkat, primary T cells and BJ-5ta fibroblasts using the RNeasy Plus Mini Kit (Qiagen, #74136), reverse transcribed to first-strand cDNAs using an iScript™ cDNA Synthesis Kit (Bio-Rad, #1708891) and analyzed by Real-time quantitative PCR (RT-qPCR) on 96-well optical PCR plates (Sarstedt) using the SsoFast™ EvaGreen® Supermix (Bio-Rad, #1725204) and specific primers for human transcripts listed in Table S1. The abundance of analyzed transcripts was determined using the ΔΔCt method and normalized to *HPRT1*.

Cell lysis, immunoblots and co-immunoprecipitation experiments

Cells (2×10^6/sample for immunoblot analysis on total cell lysates) were lysed in 1% (v/v) Triton X-100 in 20 mM Tris-HCl (pH 8), 150 mM NaCl in the presence of Protease Inhibitor Cocktail Set III (Calbiochem®, Merck, #539-134) and 0.2 mg sodium orthovanadate/ml for 5 min on ice. Protein extracts were quantified with a Quantum Protein Assay Kit

Journal of Cell Science (2021) 134, jcs258462. doi:10.1242/jcs.258462

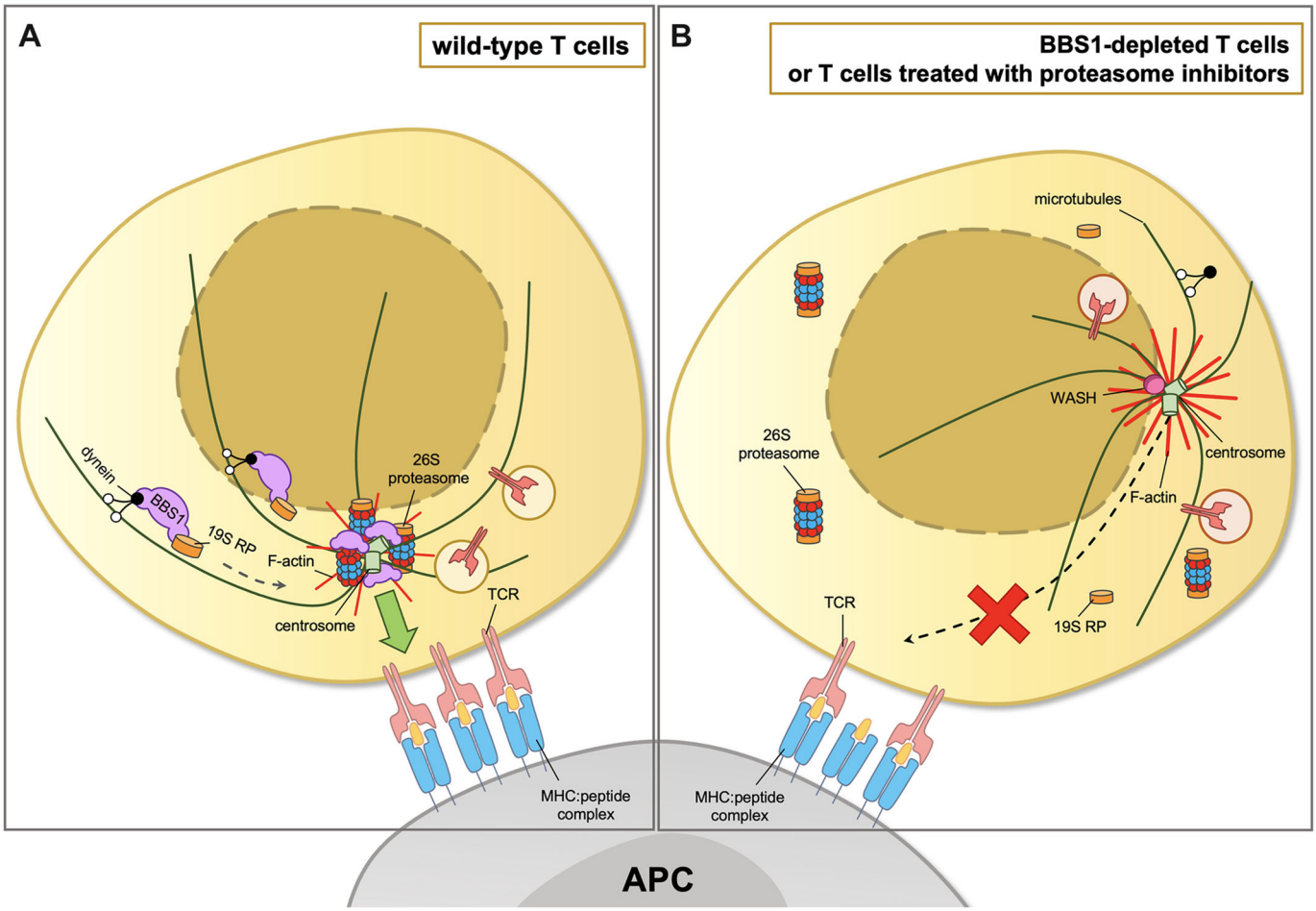

Fig. 8. Proposed model of regulation of centrosome polarization by BBS1 during T cell IS assembly. (A) BBS1 controls centrosome polarization during IS assembly by promoting the dynein-dependent recruitment of the 19S RP to the centrosome, allowing for the proteasome-regulated clearance of centrosome-associated F-actin. (B) In T cells depleted of BBS1 or treated with proteasome inhibitors, the centrosome does not polarize to the IS because of defective depletion of centrosomal F-actin.

(Euroclone, #EMP014500) and denatured in 4× Bolt™ LDS Sample Buffer (Invitrogen™, ThermoFisher Scientific, #B0007) supplemented with 10× Bolt™ Sample Reducing Buffer (Invitrogen™, #B009) for 5 min at 100°C. Proteins (10 µg) were separated on Bolt™ Bis-Tris Mini Protein Gels (Invitrogen™) or home-made gels and transferred to nitrocellulose (GE HealthCare, #GE10600002) or polyvinylidene difluoride membranes (GE HealthCare, #10600023) under wet conditions. Blocking was performed in 5% non-fat dry milk in PBS containing 0.02% Tween 20. Membranes were incubated in primary antibodies for 1–3 h at room temperature or overnight at 4°C followed by incubation in 20 ng/ml HRP-conjugated secondary antibodies (Jackson ImmunoResearch Laboratories) for 45 min at room temperature. Secondary antibodies were detected using SuperSignal™ West Pico Plus Chemiluminescent Substrates (Life Technologies, #34578). Membranes were stripped with ReBlot Plus Mild Antibody Stripping Solution 10× (Chemicon®, Merck, #2502) and reprobed with a primary antibody. For quantification, blots were scanned using a laser densitometer (DuoScan T2500, Agfa) and densitometric levels were measured using ImageJ software.

For co-immunoprecipitation (IP) experiments, cells (8–10×10^6 cells/sample) were lysed in 0.5% (v/v) Triton X-100 in 20 mM Tris-HCl (pH 8), 150 mM NaCl in the presence of Protease Inhibitor Cocktail Set III (Calbiochem®, #539-134) and 0.2 mg sodium orthovanadate/ml for 5 min on ice. Postnuclear supernatants were incubated with 3 µg Protein A Sepharose CL-4B (PAS; GE Healthcare, #GEH17078001) for 1 h at 4°C. PAS was pelleted by centrifugation (PAS controls) and supernatants were transferred to new tubes and incubated with 3 µg PAS plus primary antibody (0.4 µg anti-GFP mAb, 1.5 µg anti-Rpt2, 2 µg anti-γ-tubulin) for 2 h at 4°C. PAS controls and PAS–antibody complexes were then washed four times in IP lysis buffer. The immunoprecipitates were eluted in 2× Bolt™ LDS Sample Buffer supplemented with 10× Bolt™ Sample Reducing Buffer (Life Technologies, #B009), boiled for 5 min and resolved by SDS-PAGE. A fraction (10 µg) of the lysates used for co-IPs was run on the same gel to identify the migration of the specific immunoreactive bands.

Flow cytometry

Flow cytometry analysis of surface CD3 was carried out on control or BBS1 KD/KO Jurkat cells incubated on ice for 40 min with phycoerythrin (PE)-labelled anti-human CD3ε (OKT3; Table S2). Samples were acquired with a Guava easyCyte cytometer (Millipore) and plotted using FlowJo software (TreeStar Inc., Ashland, OR). To quantify the proportion of CD3 detectable at the cell surface in control cells untreated or treated with the proteasome inhibitors MG132 and epoxomicin, either intact or permeabilized cells were stained with PE-labelled anti-human CD3ε (Table S2).

In the reconstitution experiments, the percentage of live GFP^+ and propidium $iodide^-$ cells was determined by flow cytometry by labeling transfected cells with 0.5 µg/ml of propidium iodide (Merck, #537059).

Protein tyrosine phosphorylation was analyzed by flow cytometry in conjugates of control or BBS1 KO Jurkat cells and SEE-pulsed Vybrant™ DiO (ThermoFisher Scientific, #V22886)-labelled Raji cells (APCs) at different time points after conjugate formation. Conjugates were co-stained with an anti-p-Tyr antibody (Table S2) and DiO-negative cells were analyzed.

Statistics and reproducibility

Each experiment was performed ≥3 independent times. The exact number of repeats and the number of cells analyzed is specified in figure legends. Statistical analyses were performed using Prism software (GraphPad Software). Pairwise or multiple comparisons of values with normal distribution were carried out using Student's *t*-test (paired or unpaired), one-sample *t*-test (theoretical mean=1) and one-way ANOVA, whereas values without Gaussian distribution were analyzed with Mann–Whitney test or Kruskal–Wallis test. Statistical significance was defined as: ****$P \leq 0.0001$; ***$P \leq 0.001$; **$P \leq 0.01$; *$P \leq 0.05$; n.s., not significant.

Acknowledgements

We wish to thank Max Nachury, Valentina Cianfanelli, Federico Galvagni, Maria Isabel Yuseff and Stefan Balint for reagents and helpful suggestions, and Claire Hivroz for critical reading of the manuscript.

Competing interests

The authors declare no competing or financial interests.

Author contributions

Conceptualization: C.C., A.O., M.L.D., C.T.B.; Methodology: C.C., A.O.; Formal analysis: C.C., A.O.; Investigation: C.C., A.O., F.F., N.C., J.B., E.B.C., V.N.; Writing - original draft: C.C., A.O., C.T.B.; Writing - review & editing: F.F., N.C., E.B.C., V.N.; O.S., M.L.D.; Supervision: V.N.; O.S., M.L.D., C.T.B.; Funding acquisition: O.S., M.L.D., C.T.B.

Funding

This work was carried out with the support of Fondazione Telethon, Italy (grant GGP16003 to C.T.B). The support of the Associazione Italiana per la Ricerca sul Cancro (IG-2017-20148 to C.T.B.), the European Research Council (Synergy grant 951329 to C.T.B. and M.L.D.) and the Grantová Agentura České Republiky (19-03435Y to O.S.) is also acknowledged.

Peer review history

The peer review history is available online at https://journals.biologists.com/jcs/article-lookup/doi/10.1242/jcs.258462

References

Alcover, A., Alarcón, B. and Di Bartolo, V. (2018). Cell biology of T cell receptor expression and regulation. *Annu. Rev. Immunol.* **36**, 103-125. doi:10.1146/annurev-immunol-042617-053429

Baldari, C. T. and Rosenbaum, J. (2010). Intraflagellar transport: it's not just for cilia anymore. *Curr. Opin. Cell Biol.* **22**, 75-80. doi:10.1016/j.ceb.2009.10.010

Baldari, C. T., Macchia, G. and Telford, J. L. (1992). Interleukin-2 promoter activation in T-cells expressing activated Ha-ras. *J. Biol. Chem.* **267**, 4289-4291. doi:10.1016/S0021-9258(18)42829-3

Bard, J. A. M., Goodall, E. A., Greene, E. R., Jonsson, E., Dong, K. C. and Martin, A. (2018). Structure and function of the 26S proteasome. *Annu. Rev. Biochem.* **87**, 697-724. doi:10.1146/annurev-biochem-062917-011931

Bello-Gamboa, A., Velasco, M., Moreno, S., Herranz, G., Ilie, R., Huetos, S., Dávila, S., Sáncheza, A., De La Serna, J. B., Calvo, V. et al. (2020). Actin reorganization at the centrosomal area and the immune synapse regulates polarized secretory traffic of multivesicular bodies in T lymphocytes. *J. Extracell. Vesicles* **9**, 1759926. doi:10.1080/20013078.2020.1759926

Bjornson-Hooper, Z. B., Fragiadakis, G. K., Spitzer, M. H., Madhireddy, D., McIlwain, D. and Nolan, G. P. (2019). A comprehensive atlas of immunological differences between humans, mice and non-human primates. *bioRxiv* doi:10.1101/574160

Bonello, G., Blanchard, N., Montoya, M. C., Aguado, E., Langlet, C., He, H.-T., Nunez-Cruz, S., Malissen, M., Sanchez-Madrid, F., Olive, D. et al. (2004). Dynamic recruitment of the adaptor protein LAT: LAT exists in two distinct intracellular pools and controls its own recruitment. *J. Cell Sci.* **117**, 1009-1016. doi:10.1242/jcs.00968

Bouchet, J., Del Río-Iñiguez, I., Lasserre, R., Agüera-Gonzalez, S., Cuche, C., Danckaert, A., McCaffrey, M. W., Di Bartolo, V. and Alcover, A. (2016). Rac1-Rab11-FIP3 regulatory hub coordinates vesicle traffic with actin remodeling and T-cell activation. *EMBO J.* **35**, 1160-1174. doi:10.15252/embj.201593274

Burakov, A. V. and Nadezhdina, E. S. (2013). Association of nucleus and centrosome: magnet or velcro? *Cell Biol. Int.* **37**, 95-104. doi:10.1002/cbin.10016

Bustos-Morán, E., Blas-Rus, N., Martín-Cófreces, N. B. and Sánchez-Madrid, F. (2016). Orchestrating lymphocyte polarity in cognate immune cell-cell interactions. *Int. Rev. Cell Mol. Biol.* **327**, 195-261. doi:10.1016/bs.ircmb.2016.06.004

Capitani, N., Onnis, A., Finetti, F., Cassioli, C., Plebani, A., Brunetti, J., Troilo, A., D'Elios, S., Baronio, M., Gazzurelli, L. et al. (2021). A CVID-associated variant in the ciliogenesis protein CCDC28B disrupts immune synapse assembly. *Cell Death Differ*. doi:10.1038/s41418-021-00837-5

Cassioli, C. and Baldari, C. T. (2019). A ciliary view of the immunological synapse. *Cells* **8**, 789. doi:10.3390/cells8080789

Chicaybam, L., Sodre, A. L., Curzio, B. A. and Bonamino, M. H. (2013). An efficient low cost method for gene transfer to T lymphocytes. *PLoS ONE* **8**, e60298. doi:10.1371/journal.pone.0060298

Choudhuri, K., Llodrá, J., Roth, E. W., Tsai, J., Gordo, S., Wucherpfennig, K. W., Kam, L. C., Stokes, D. L. and Dustin, M. L. (2014). Polarized release of T-cell-receptor-enriched microvesicles at the immunological synapse. *Nature* **507**, 118-123. doi:10.1038/nature12951

Compeer, E. B., Kraus, F., Ecker, M., Redpath, G., Amiezer, M., Rother, N., Nicovich, P. R., Kapoor-Kaushik, N., Deng, Q., Samson, G. P. B. et al. (2018). A mobile endocytic network connects clathrin-independent receptor endocytosis to recycling and promotes T cell activation. *Nat. Commun.* **9**, 1597. doi:10.1038/s41467-018-04088-w

Das, V., Nal, B., Dujeancourt, A., Thoulouze, M.-I., Galli, T., Roux, P., Dautry-Varsat, A. and Alcover, A. (2004). Activation-induced polarized recycling targets T cell antigen receptors to the immunological synapse: involvement of SNARE complexes. *Immunity* **20**, 577-588. doi:10.1016/S1074-7613(04)00106-2

de la Roche, M., Ritter, A. T., Angus, K. L., Dinsmore, C., Earnshaw, C. H., Reiter, J. F. and Griffiths, G. M. (2013). Hedgehog signaling controls T cell killing at the immunological synapse. *Science* **342**, 1247-1250. doi:10.1126/science.1244689

de la Roche, M., Asano, Y. and Griffiths, G. M. (2016). Origins of the cytolytic synapse. *Nat. Rev. Immunol.* **16**, 421-432. doi:10.1038/nri.2016.54

Desai, P. B., Stuck, M. W., Lv, B. and Pazour, G. J. (2020). Ubiquitin links smoothened to intraflagellar transport to regulate Hedgehog signaling. *J. Cell Biol.* **219**, e201912104. doi:10.1083/jcb.201912104

Didier, C., Merdes, A., Gairin, J.-E. and Jabrane-Ferrat, N. (2008). Inhibition of proteasome activity impairs centrosome-dependent microtubule nucleation and organization. *Mol. Biol. Cell* **19**, 1220-1229. doi:10.1091/mbc.e06-12-1140

Dustin, M. L. (2014). The immunological synapse. *Cancer Immunol. Res.* **2**, 1023-1033. doi:10.1158/2326-6066.CIR-14-0161

Ehrlich, L. I. R., Ebert, P. J. R., Krummel, M. F., Weiss, A. and Davis, M. M. (2002). Dynamics of p56lck translocation to the T cell immunological synapse following agonist and antagonist stimulation. *Immunity* **17**, 809-822. doi:10.1016/S1074-7613(02)00481-8

Farina, F., Gaillard, J., Guérin, C., Couté, Y., Sillibourne, J., Blanchoin, L. and Théry, M. (2016). The centrosome is an actin-organizing centre. *Nat. Cell Biol.* **18**, 65-75. doi:10.1038/ncb3285

Finetti, F., Paccani, S. R., Riparbelli, M. G., Giacomello, E., Perinetti, G., Pazour, G. J., Rosenbaum, J. L. and Baldari, C. T. (2009). Intraflagellar transport is required for polarized recycling of the TCR/CD3 complex to the immune synapse. *Nat. Cell Biol.* **11**, 1332-1339. doi:10.1038/ncb1977

Finetti, F., Patrussi, L., Masi, G., Onnis, A., Galgano, D., Lucherini, O. M., Pazour, G. J. and Baldari, C. T. (2014). Specific recycling receptors are targeted to the immune synapse by the intraflagellar transport system. *J. Cell Sci.* **127**, 1924-1937. doi:10.1242/jcs.139337

Finetti, F., Patrussi, L., Galgano, D., Cassioli, C., Perinetti, G., Pazour, G. J. and Baldari, C. T. (2015). The small GTPase Rab8 interacts with VAMP-3 to regulate the delivery of recycling T-cell receptors to the immune synapse. *J. Cell Sci.* **128**, 2541-2552. doi:10.1242/jcs.171652

Finetti, F., Cassioli, C. and Baldari, C. T. (2017). Transcellular communication at the immunological synapse: a vesicular traffic-mediated mutual exchange. *F1000Research* **6**, 1880. doi:10.12688/f1000research.11944.1

Follit, J. A., Tuft, R. A., Fogarty, K. E. and Pazour, G. J. (2006). The intraflagellar transport protein IFT20 is associated with the Golgi complex and is required for cilia assembly. *Mol. Biol. Cell* **17**, 3781-3792. doi:10.1091/mbc.e06-02-0133

Forsythe, E. and Beales, P. L. (2013). Bardet-Biedl syndrome. *Eur. J. Hum. Genet.* **21**, 8-13. doi:10.1038/ejhg.2012.115

Galgano, D., Onnis, A., Pappalardo, E., Galvagni, F., Acuto, O. and Baldari, C. T. (2017). The T cell IFT20 interactome reveals new players in immune synapse assembly. *J. Cell Sci.* **130**, 1120-1121. doi:10.1242/jcs.200006

Gawden-Bone, C. M., Frazer, G. L., Richard, A. C., Ma, C. Y., Strege, K. and Griffiths, G. M. (2018). PIP5 Kinases regulate membrane phosphoinositide and actin composition for targeted granule secretion by cytotoxic lymphocytes. *Immunity* **49**, 427-437.e4. doi:10.1016/j.immuni.2018.08.017

Gomez, T. S. and Billadeau, D. D. (2009). A FAM21-containing WASH complex regulates retromer-dependent sorting. *Dev. Cell* **17**, 699-711. doi:10.1016/j.devcel.2009.09.009

Guo, D.-F., Cui, H., Zhang, Q., Morgan, D. A., Thedens, D. R., Nishimura, D., Grobe, J. L., Sheffield, V. C. and Rahmouni, K. (2016). The BBSome controls energy homeostasis by mediating the transport of the leptin receptor to the plasma membrane. *PLoS Genet.* **12**, e1005890. doi:10.1371/journal.pgen.1005890

Haeussler, M., Schönig, K., Eckert, H., Eschstruth, A., Mianné, J., Renaud, J.-B., Schneider-Maunoury, S., Shkumatava, A., Teboul, L., Kent, J. et al. (2016). Evaluation of off-target and on-target scoring algorithms and integration into the

guide RNA selection tool CRISPOR. *Genome Biol.* **17**, 148. doi:10.1186/s13059-016-1012-2

Hao, Y.-H., Doyle, J. M., Ramanathan, S., Gomez, T. S., Jia, D., Xu, M., Chen, Z. J., Billadeau, D. D., Rosen, M. K. and Potts, P. R. (2013). Regulation of WASH-dependent actin polymerization and protein trafficking by ubiquitination. *Cell* **152**, 1051-1064. doi:10.1016/j.cell.2013.01.051

Hsu, M.-T., Guo, C.-L., Liou, A. Y., Chang, T.-Y., Ng, M.-C., Florea, B. I., Overkleeft, H. S., Wu, Y.-L., Liao, J.-C. and Cheng, P.-L. (2015). Stage-dependent axon transport of proteasomes contributes to axon development. *Dev. Cell* **35**, 418-431. doi:10.1016/j.devcel.2015.10.018

Ibañez-Vega, J., Del Valle Batalla, F., Saez, J. J., Soza, A. and Yuseff, M.-I. (2019). Proteasome dependent actin remodeling facilitates antigen extraction at the immune synapse of B cells. *Front. Immunol.* **10**, 225. doi:10.3389/fimmu.2019.00225

Jin, H., White, S. R., Shida, T., Schulz, S., Aguiar, M., Gygi, S. P., Bazan, J. F. and Nachury, M. V. (2010). The conserved Bardet-Biedl syndrome proteins assemble a coat that traffics membrane proteins to cilia. *Cell* **141**, 1208-1219. doi:10.1016/j.cell.2010.05.015

Joseph, N., Biber, G., Fried, S., Reicher, B., Levy, O., Sabag, B., Noy, E. and Barda-Saad, M. (2017). A conformational change within the WAVE2 complex regulates its degradation following cellular activation. *Sci. Rep.* **7**, 44863. doi:10.1038/srep44863

Katsanis, N. (2004). The oligogenic properties of Bardet-Biedl syndrome. *Hum. Mol. Genet.* **13** Suppl. 1, R65-R71. doi:10.1093/hmg/ddh092

Langousis, G., Shimogawa, M. M., Saada, E. A., Vashisht, A. A., Spreafico, R., Nager, A. R., Barshop, W. D., Nachury, M. V., Wohlschlegel, J. A. and Hill, K. L. (2016). Loss of the BBSome perturbs endocytic trafficking and disrupts virulence of *Trypanosoma brucei*. *Proc. Natl. Acad. Sci. USA* **113**, 632-637. doi:10.1073/pnas.1518079113

Larghi, P., Williamson, D. J., Carpier, J.-M., Dogniaux, S., Chemin, K., Bohineust, A., Danglot, L., Gaus, K., Galli, T. and Hivroz, C. (2013). VAMP7 controls T cell activation by regulating the recruitment and phosphorylation of vesicular Lat at TCR-activation sites. *Nat. Immunol.* **14**, 723-731. doi:10.1038/ni.2609

Liu, Y. P., Tsai, I.-C., Morleo, M., Oh, E. C., Leitch, C. C., Massa, F., Lee, B.-H., Parker, D. S., Finley, D., Zaghlou, N. A. et al. (2014). Ciliopathy proteins regulate paracrine signaling by modulating proteasomal degradation of mediators. *J. Clin. Investig.* **124**, 2059-2070. doi:10.1172/JCI71898

Lui-Roberts, W. W. Y., Stinchcombe, J. C., Ritter, A. T., Akhmanova, A., Karakesisoglou, I. and Griffiths, G. M. (2012). Cytotoxic T lymphocyte effector function is independent of nucleus-centrosome dissociation. *Eur. J. Immunol.* **42**, 2132-2141. doi:10.1002/eji.201242525

Manders, E. M., Stap, J., Brakenhoff, G. J., van Driel, R. and Aten, J. A. (1992). Dynamics of three-dimensional replication patterns during the S-phase, analysed by double labelling of DNA and confocal microscopy. *J. Cell Sci.* **103**, 857-862. doi:10.1242/jcs.103.3.857

Martín-Cófreces, N. B., Robles-Valero, J., Cabrero, J. R., Mittelbrunn, M., Gordón-Alonso, M., Sung, C.-H., Alarcon, B., Vázquez, J. and Sánchez-Madrid, F. (2008). MTOC translocation modulates IS formation and controls sustained T cell signaling. *J. Cell Biol.* **182**, 951-962. doi:10.1083/jcb.200801014

Martín-Cófreces, N. B., Baixauli, F., López, M. J., Gil, D., Monjas, A., Alarcón, B. and Sánchez-Madrid, F. (2012). End-binding protein 1 controls signal propagation from the T cell receptor. *EMBO J.* **31**, 4140-4152. doi:10.1038/emboj.2012.242

Martin-Cofreces, N. B., Chichon, F. J., Calvo, E., Torralba, D., Bustos-Moran, E., Dosil, S. G., Rojas-Gomez, A., Bonzon-Kulichenko, E., Lopez, J. A., Otón, J. et al. (2020). The chaperonin CCT controls T cell receptor-driven 3D configuration of centrioles. *Sci. Adv.* **6**, eabb7242. doi:10.1126/sciadv.abb7242

Mestas, J. and Hughes, C. C. W. (2004). Of mice and not men: differences between mouse and human immunology. *J. Immunol.* **172**, 2731-2738. doi:10.4049/jimmunol.172.5.2731

Mourão, A., Nager, A. R., Nachury, M. V. and Lorentzen, E. (2014). Structural basis for membrane targeting of the BBSome by ARL6. *Nat. Struct. Mol. Biol.* **21**, 1035-1041. doi:10.1038/nsmb.2920

Mourão, A., Christensen, S. T. and Lorentzen, E. (2016). Corrigendum to "The intraflagellar transport machinery in ciliary signaling" [Curr Opin Struct Biol 2016, 41:98–108]. *Curr. Opin. Struct. Biol.* **41**, 255. doi:10.1016/j.sbi.2016.07.018

Nachury, M. V. (2018). The molecular machines that traffic signaling receptors into and out of cilia. *Curr. Opin. Cell Biol.* **51**, 124-131. doi:10.1016/j.ceb.2018.03.004

Nakayama, K. and Katoh, Y. (2018). Ciliary protein trafficking mediated by IFT and BBSome complexes with the aid of kinesin-2 and dynein-2 motors. *J. Biochem.* **163**, 155-164. doi:10.1093/jb/mvx087

Nath, S., Christian, L., Tan, S. Y., Ki, S., Ehrlich, L. I. R. and Poenie, M. (2016). dynein separately partners with NDE1 and dynactin to orchestrate T cell focused secretion. *J. Immunol.* **197**, 2090-2101. doi:10.4049/jimmunol.1600180

Nozaki, S., Katoh, Y., Kobayashi, T. and Nakayama, K. (2018). BBS1 is involved in retrograde trafficking of ciliary GPCRs in the context of the BBSome complex. *PLoS ONE* **13**, e0195005. doi:10.1371/journal.pone.0195005

Obino, D., Farina, F., Malbec, O., Sáez, P. J., Maurin, M., Gaillard, J., Dingli, F., Loew, D., Gautreau, A., Yuseff, M.-I. et al. (2016). Actin nucleation at the centrosome controls lymphocyte polarity. *Nat. Commun.* **7**, 10969. doi:10.1038/ncomms10969

Onnis, A. and Baldari, C. T. (2019). Orchestration of immunological synapse assembly by vesicular trafficking. *Front. Cell Dev. Biol.* **7**, 110. doi:10.3389/fcell.2019.00110

Onnis, A., Finetti, F., Patrussi, L., Gottardo, M., Cassioli, C., Spanò, S. and Baldari, C. T. (2015). The small GTPase Rab29 is a common regulator of immune synapse assembly and ciliogenesis. *Cell Death Differ.* **22**, 1687-1699. doi:10.1038/cdd.2015.17

Pedersen, L. B. and Rosenbaum, J. L. (2008). Intraflagellar transport (IFT): role in ciliary assembly, resorption and signalling. *Curr. Top. Dev. Biol.* **85**, 23-61. doi:10.1016/S0070-2153(08)00802-8

Prasai, A., Schmidt Cernohorska, M., Ruppova, K., Niederlova, V., Andelova, M., Draber, P., Stepanek, O. and Huranova, M. (2020). The BBSome assembly is spatially controlled by BBS1 and BBS4 in human cells. *J. Biol. Chem.* **295**, 14279-14290. doi:10.1074/jbc.RA120.013905

Ran, F. A., Hsu, P. D., Wright, J., Agarwala, V., Scott, D. A. and Zhang, F. (2013). Genome engineering using the CRISPR-Cas9 system. *Nat. Protoc.* **8**, 2281-2308. doi:10.1038/nprot.2013.143

Roy, N. H. and Burkhardt, J. K. (2018). The actin cytoskeleton: a mechanical intermediate for signal integration at the immunological synapse. *Front. Cell Dev. Biol.* **6**, 116. doi:10.3389/fcell.2018.00116

Seaman, M. N. J., Gautreau, A. and Billadeau, D. D. (2013). Retromer-mediated endosomal protein sorting: all WASHed up!. *Trends Cell Biol.* **23**, 522-528. doi:10.1016/j.tcb.2013.04.010

Soares, H., Lasserre, R. and Alcover, A. (2013). Orchestrating cytoskeleton and intracellular vesicle traffic to build functional immunological synapses. *Immunol. Rev.* **256**, 118-132. doi:10.1111/imr.12110

Starks, R. D., Beyer, A. M., Guo, D. F., Boland, L., Zhang, Q. H., Sheffield, V. C. and Rahmouni, K. (2015). Regulation of insulin receptor trafficking by bardet biedl syndrome proteins. *PLoS Genet.* **11**, e1005311. doi:10.1371/journal.pgen.1005311

Stephen, L. A., ElMaghloob, Y., McIlwraith, M. J., Yelland, T., Castro Sanchez, P., Roda-Navarro, P. and Ismail, S. (2018). The ciliary machinery is repurposed for T cell immune synapse trafficking of LCK. *Dev. Cell* **47**, 122-132.e4. doi:10.1016/j.devcel.2018.08.012

Stinchcombe, J. C. and Griffiths, G. M. (2014). Communication, the centrosome and the immunological synapse. *Philos. Trans. R. Soc. Biol. Sci.* **369**, 20130463. doi:10.1098/rstb.2013.0463

Tobin, J. L. and Beales, P. L. (2009). The nonmotile ciliopathies. *Genet. Med.* **11**, 386-402. doi:10.1097/GIM.0b013e3181a02882

Tsang, S. H., Aycinena, A. R. P. and Sharma, T. (2018). Ciliopathy: bardet-biedl syndrome. *Adv. Exp. Med. Biol.* **1085**, 171-174. doi:10.1007/978-3-319-95046-4_33

Tsyklauri, O., Niederlova, V., Forsythe, E., Prasai, A., Drobek, A., Kasparek, P., Sparks, K., Trachtulec, Z., Prochazka, J., Sedlacek, R. et al. (2021). Bardet-Biedl Syndrome ciliopathy is linked to altered hematopoiesis and dysregulated self-tolerance. *EMBO Rep.* **22**, e50785.

Vardhana, S., Choudhuri, K., Varma, R. and Dustin, M. L. (2010). Essential role of ubiquitin and TSG101 protein in formation and function of the central supramolecular activation cluster. *Immunity* **32**, 531-540. doi:10.1016/j.immuni.2010.04.005

Vora, S. M. and Phillips, B. T. (2016). The benefits of local depletion: the centrosome as a scaffold for ubiquitin-proteasome-mediated degradation. *Cell Cycle* **15**, 2124-2134. doi:10.1080/15384101.2016.1196306

Walczak, H., Iwai, K. and Dikic, I. (2012). Generation and physiological roles of linear ubiquitin chains. *BMC Biol.* **10**, 23. doi:10.1186/1741-7007-10-23

Wang, J., Fedoseienko, F., Chen, B., Burstein, E., Jia, D. and Billadeau, D. D. (2018). Endosomal receptor trafficking: retromer and beyond. *Traffic* **19**, 578-590. doi:10.1111/tra.12574

Watanabe, Y., Sasahara, Y., Ramesh, N., Massaad, M. J., Yeng Looi, C., Kumaki, S., Kure, S., Geha, R. S. and Tsuchiya, S. (2013). T-cell receptor ligation causes Wiskott-Aldrich syndrome protein degradation and F-actin assembly downregulation. *J. Allergy Clin. Immunol.* **132**, 648-655.e1. doi:10.1016/j.jaci.2013.03.046

Wingfield, J. L., Lechtreck, K.-F. and Lorentzen, E. (2018). Trafficking of ciliary membrane proteins by the intraflagellar transport/BBSome machinery. *Essays Biochem.* **62**, 753-763. doi:10.1042/EBC20180030

Xu, Q., Zhang, Y., Wei, Q., Huang, Y., Li, Y., Ling, K. and Hu, J. (2015). BBS4 and BBS5 show functional redundancy in the BBSome to regulate the degradative sorting of ciliary sensory receptors. *Sci. Rep.* **5**, 11855. doi:10.1038/srep11855

Ye, F., Nager, A. R. and Nachury, M. V. (2018). BBSome trains remove activated GPCRs from cilia by enabling passage through the transition zone. *J. Cell Biol.* **217**, 1847-1868. doi:10.1083/jcb.201709041

Zucchetti, A. E., Bataille, L., Carpier, J.-M., Dogniaux, S., San Roman-Jouve, M., Maurin, M., Stuck, M. W., Rios, R. M., Baldari, C. T., Pazour, G. J. et al. (2019). Tethering of vesicles to the Golgi by GMAP210 controls LAT delivery to the immune synapse. *Nat. Commun.* **10**, 2864. doi:10.1038/s41467-019-10891-w

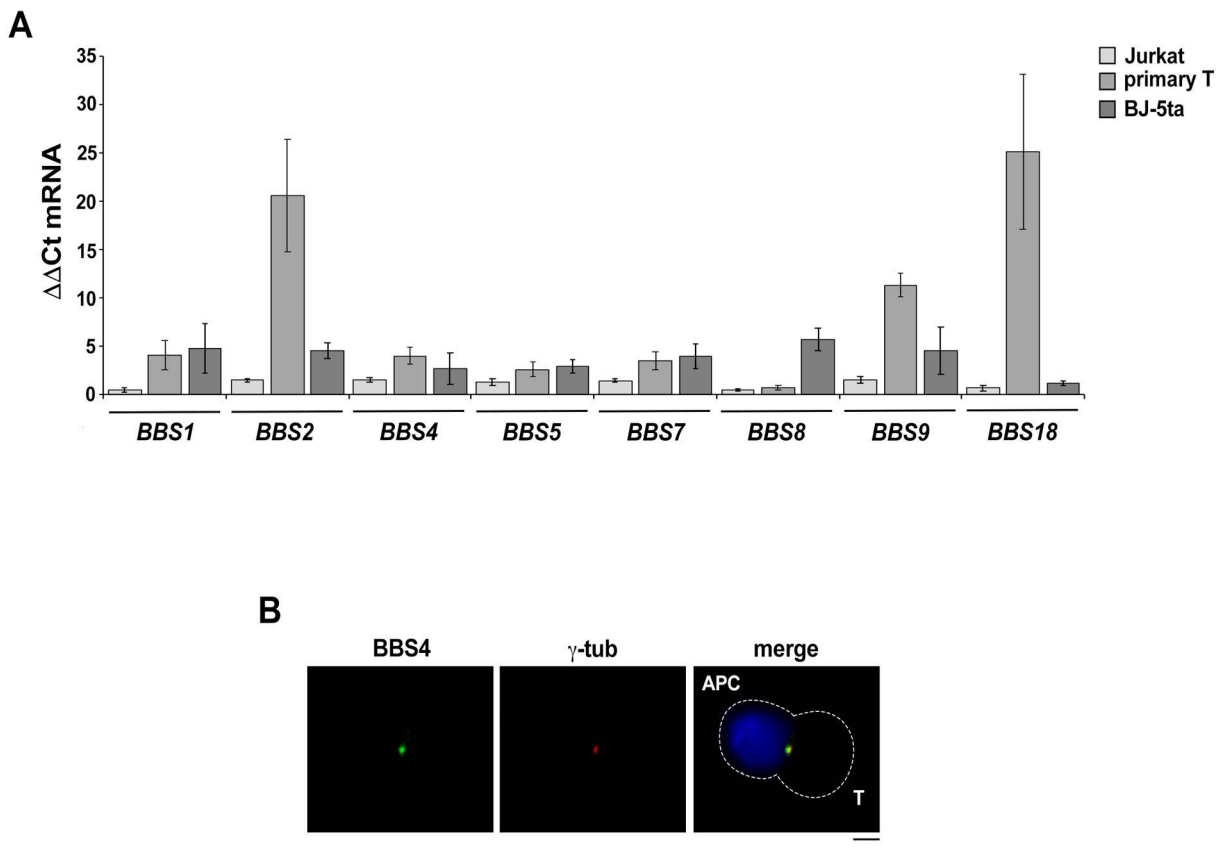

Fig. S1. T cells express all BBSome core components. (A) Real-time quantitative PCR (RT-qPCR) of the BBSome subunits *BBS-1*, *-2*, *-4*, *-5*, *-7*, *-8*, *-9* and *-18* in Jurkat cells, primary T cells and BJ-5ta cells (n≥3). The bar graph shows the abundance of analyzed transcripts, which was determined using the ΔΔCt method and normalized to *HPRT1*. (B) Immunofluorescence analysis (IF) of BBS4 in 30-min conjugates of SEE-pulsed Ramos cells (APCs) and SYFP-BBS4-expressing Jurkat cells co-stained for γ-tubulin (γ-tub). Representative images (medial optical sections) are shown. Dashed line marks the outline of the two cells. Scale bars: 5 µm.

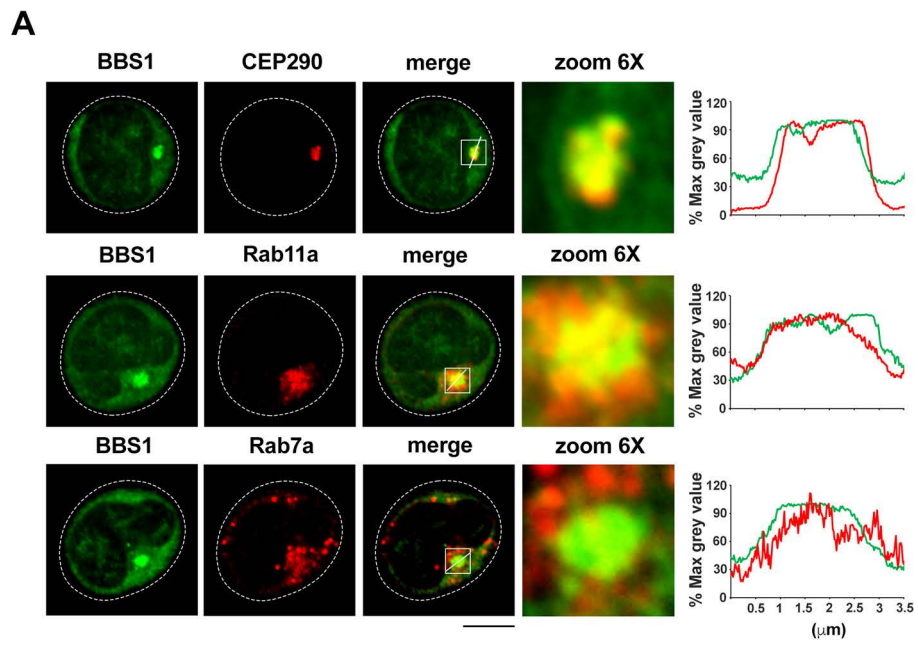

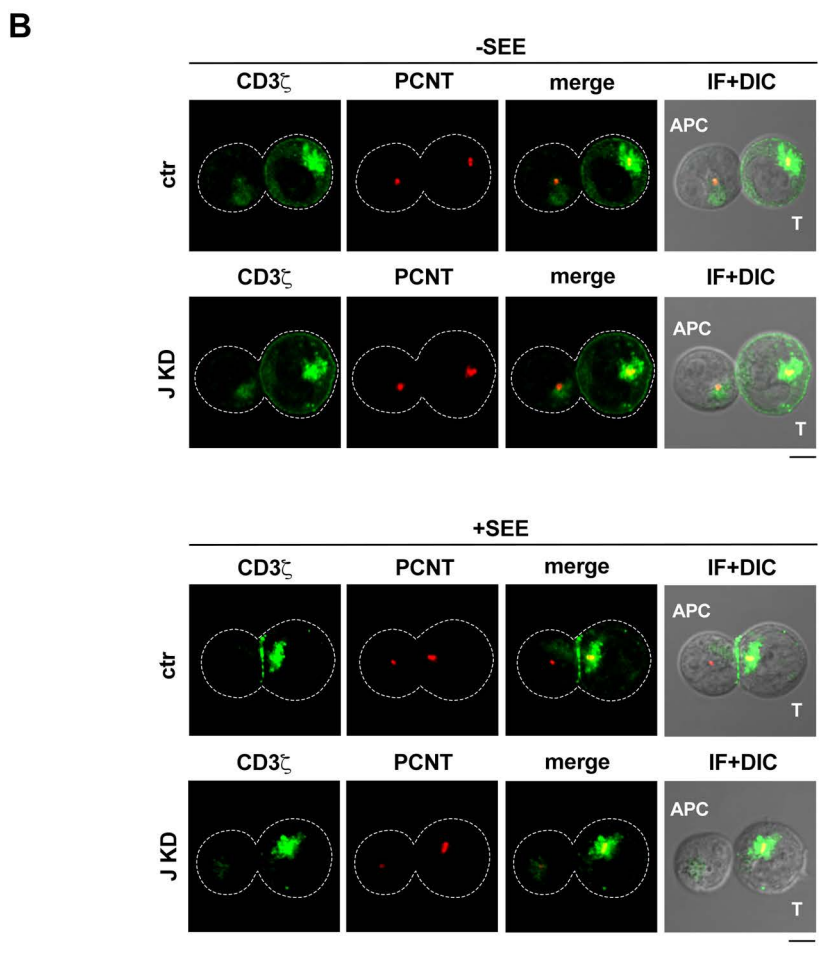

Fig. S2. Representative images of the BBS1 co-localization analyses and of conjugates stained for PCNT and CD3ζ. (A) Immunofluorescence analysis (IF) of BBS1-GFP expressing Jurkat cells co-stained for CEP290 (pericentrosomal marker), Rab11a (recycling endosomes) and Rab7a (late endosomes). Representative images (medial optical sections) are shown. Dashed lines mark the cell outline. Boxes indicate regions shown in 6X zoom images. Right: Intensity profiles along the lines within the selected areas in the overlay images for each channel are shown. Raw pixel intensity signals were normalized to maximum intensity pixel of each channel (% max grey value). Quantification (mean±s.d.) using Manders' coefficient of the weighted colocalization of GFP with these markers is shown in Fig. 1C (10 cells/sample, n≥3). (B) Immunofluorescence analysis (IF) of pericentrin (PCNT) and CD3ζ localization in 15-min conjugates of control (ctr) and BBS1KD (J KD) Jurkat cells with Raji cells (APCs) in the absence or presence of SEE (n=3). Dashed line marks the outline of the two cells. DIC, differential interference contrast. Scale bar: 5 µm.

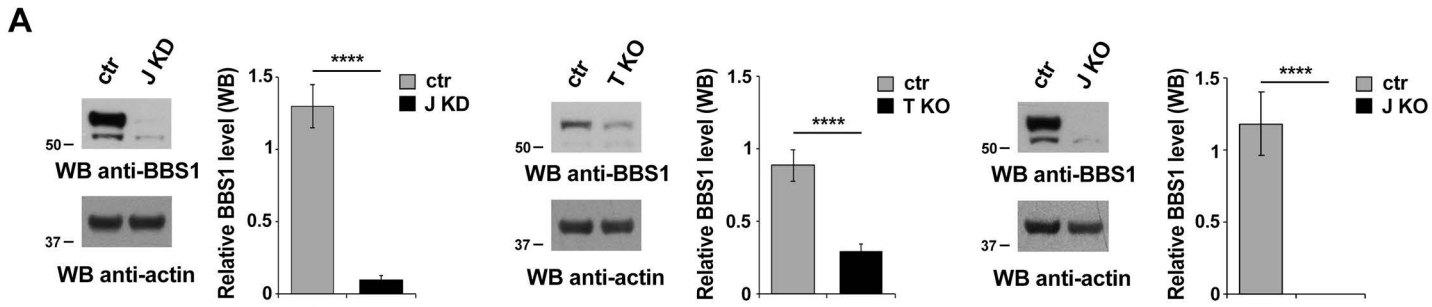

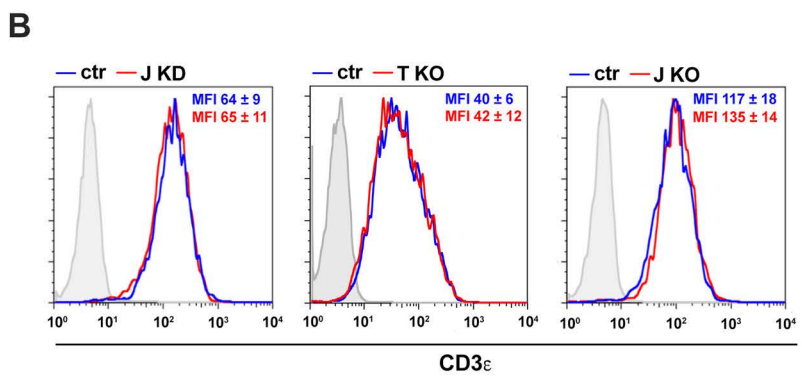

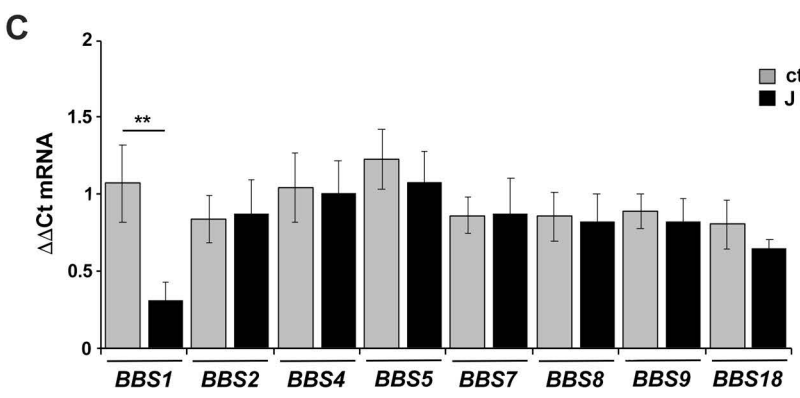

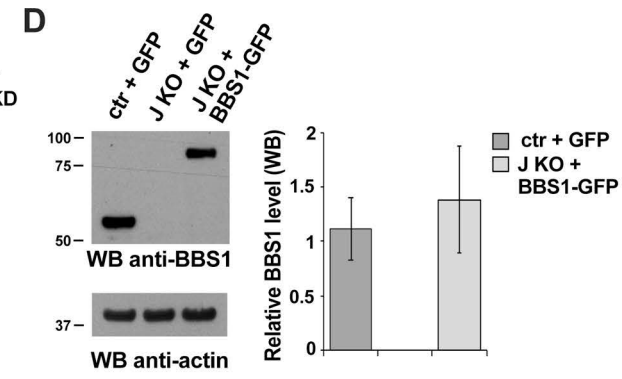

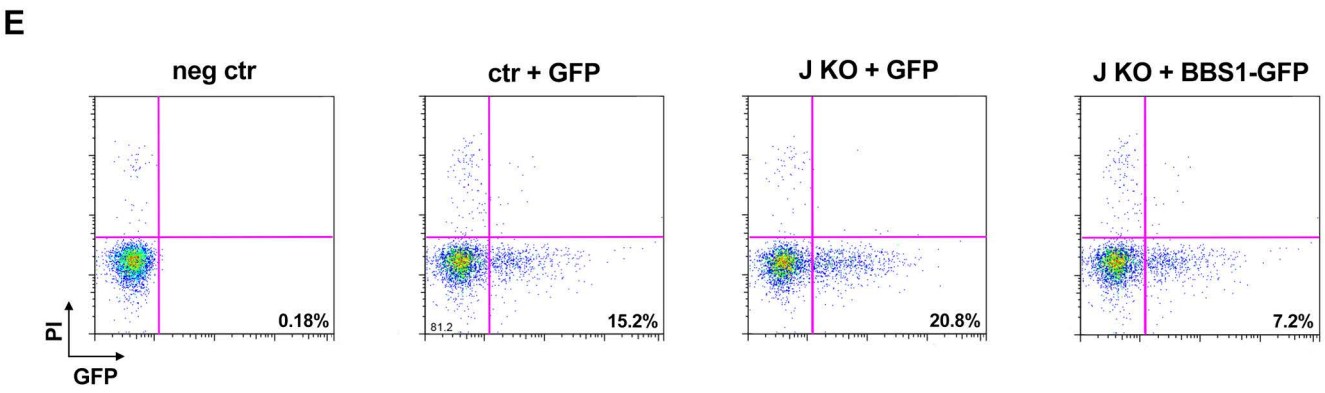

Fig. S3. Characterization of the Jurkat cell lines and primary T cells used in this study. (A) Western blot (WB) analysis of BBS1 in lysates of Jurkat cells transduced with lentiviral particles carrying a non-targeting control shRNA (ctr) or an shRNA specific for BBS1 (J KD) (left), or in lysates of control (ctr) primary and BBS1 KO (T KO) primary T cells gene-edited by CRISPR-Cas9 technology (middle), or in lysates of control (ctr) and BBS1 KO (J KO) Jurkat cells gene-edited by CRISPR-Cas9 technology (right) (n≥3). Representative immunoblots are shown. The migration of molecular mass markers is shown (kDa). The bar graphs show the relative protein expression normalized to actin (n≥3, paired two-tailed Student's *t*-test). Data are expressed as mean±s.d. (B) Flow cytometric analysis of CD3ε in Jurkat cells transduced with lentiviral particles carrying a non-targeting control shRNA (ctr) or an shRNA specific for BBS1 (J KD) (*left*), in control (ctr) and BBS1 KO (T KO) primary T cells (*middle*), or control (ctr) and BBS1 KO (J KO) Jurkat cells (*right*). The means of mean fluorescence intensities (MFIs) measured in multiple experiments are reported in each representative FACS profile (n≥3). (C) Real-time quantitative PCR (RT-qPCR) of the BBSome subunits *BBS1*, *-2*, *-4*, *-5*, *-7*, *-8*, *-9* and *-18* in control (ctr) and BBS1KD (J KD) Jurkat cells. The bar graph shows the abundance of analyzed transcripts, which was determined using the ΔΔCt method and normalized to *HPRT1*. (D) Western blot (WB) analysis of BBS1 in lysates of control (ctr) or BBS1 KO (J KO) Jurkat cells. Ctr and J KO cells were transfected with the empty vector (ctr+GFP, J KO+GFP); only J KO cells were transfected with the same vector encoding wild-type BBS1 (J KO+BBS1-GFP) (n=3). Representative immunoblots are shown. The migration of molecular mass markers is shown (kDa). Right: Bar graphs showing of the relative protein expression normalized to actin (n=3). (E) Flow cytometric analysis of GFP in control (ctr) Jurkat cells either untransfected (neg ctr) or transfected with the empty vector (ctr+GFP), and BBS1 KO (J KO) Jurkat cells transfected with either the empty vector (J KO+GFP) or the same vector encoding wild-type BBS1 (J KO+BBS1-GFP) (n=3). Cells were co-stained with the cell viability dye propidium iodide (PI) and analyzed 24 h after transfection. The percentages (%) of GFP^+ and PI^- cells are shown in each representative dot plot. Data are expressed as mean±s.d. ***P≤0.001; **P≤0.01.

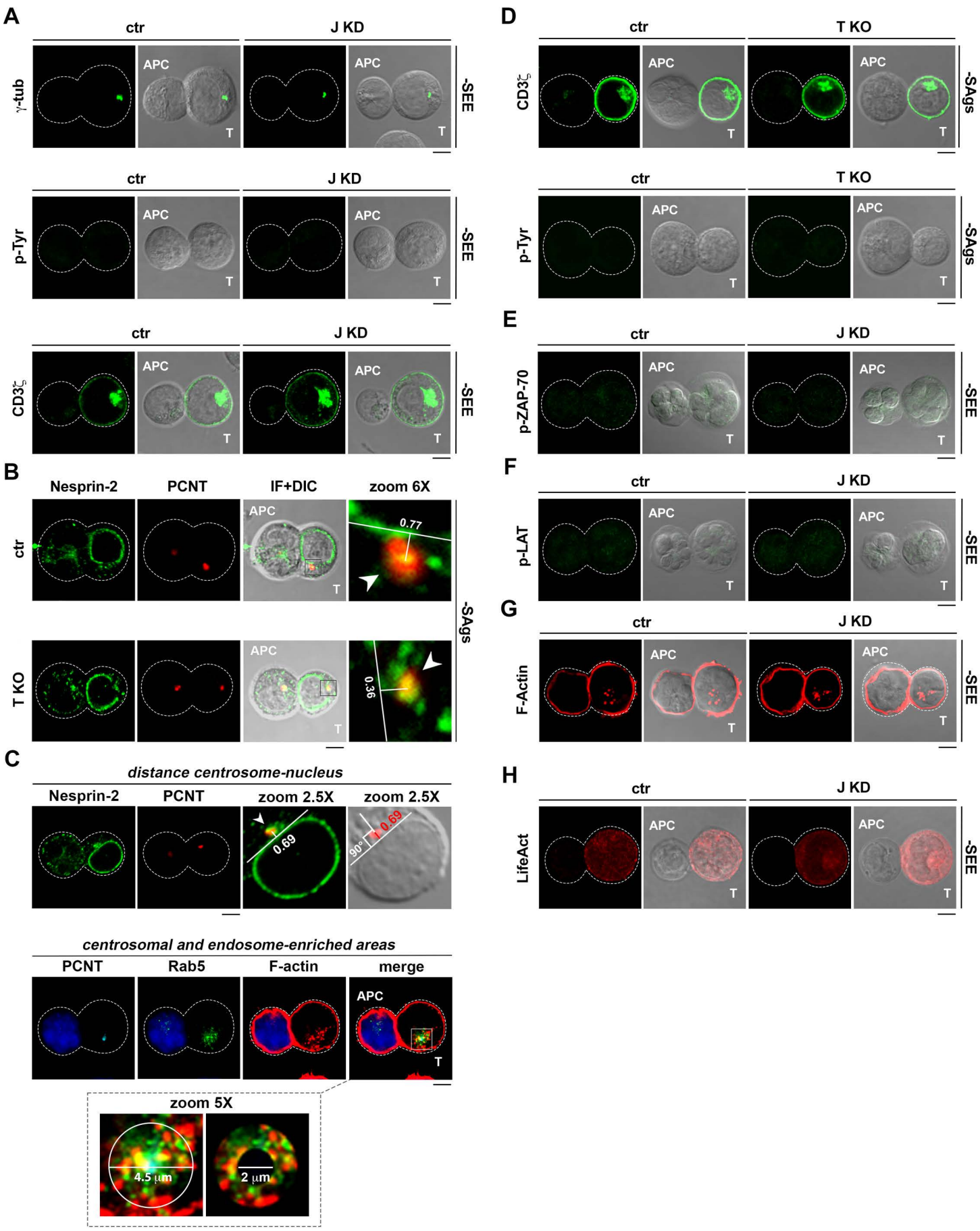
A
ctr
J KD
γ-tub
p-Tyr
CD3ζ
APC
T
-SEE
B
Nesprin-2
PCNT
IF+DIC
zoom 6X
ctr
T KO
0.77
0.36
-SAgs
C
distance centrosome-nucleus
Nesprin-2
PCNT
zoom 2.5X
zoom 2.5X
0.69
90°
centrosomal and endosome-enriched areas
PCNT
Rab5
F-actin
merge
zoom 5X
4.5 μm
2 μm
D
T KO
E
p-ZAP-70
F
p-LAT
G
F-Actin
H
LifeAct

Fig. S4. Representative images of non-activated T cell conjugates and masks for image analyses. (A) Immunofluorescence analysis (IF) of centrosome (γ–tubulin; γ-tub), CD3ζ and tyrosine phosphoproteins (p-Tyr) in conjugates of control (ctr) and BBS1KD (J KD) Jurkat cells with Raji B cells (APCs) in the absence of SEE (n≥3). Quantifications (mean±s.d.) are shown in Fig. 2C,H, Fig. 3A. (B) Immunofluorescence analysis (IF) of pericentrin (PCNT) in conjugates of control (ctr) and BBS1KO (T KO) primary T cells with Raji B cells (APCs) in the absence of SAgs. Conjugates were co-stained for Nesprin-2. Representative images (medial optical sections) are shown. Boxes indicate the regions shown in 6X zoom images. Arrowheads indicate the centrosomes and the perpendicular lines show the centrosome-nucleus distances (see Fig. S4C for quantification). DIC, differential interference contrast. Quantifications (mean±s.d.) are shown in Fig. 2D,E. (C) Top: Representative image of a T cell-APC conjugate co-stained with anti-Nesprin-2 and anti-PCNT antibodies. The T cell was magnified to highlight the parameters used for quantification. A line from the center of the centrosome (PCNT) forming an angle of 90° with the tangent to the nuclear membrane (Nesprin-2) was drawn to measure the distance between nucleus and centrosome (μm) in primary T cells. In cells showing a weak Nesprin-2 staining the centrosome-nucleus distance was further confirmed by overlaying the PCNT fluorescence to the DIC image, in which the nuclear contour is easily identified. Arrowheads indicate the centrosomes. DIC, differential interference contrast. Bottom: Representative image of Jurkat cells conjugated with Raji cells (APCs) for 15 min and triple stained for PCNT, Rab5 and F-actin. Boxes indicate the regions shown in 5X zoom images, in which the parameters used for quantification were depicted. A 2 μm diameter circle centered around the centrosome of Jurkat cells (or 1.2 μm for primary T cells) indicates the centrosomal area used for the colocalization analyses shown in Fig. 4B,D, Fig. 6I, Fig. 7A-D,G, Fig. S5F,G, Fig. S7J. The endosome-enriched ring corresponding to a 4.5 μm diameter circle around the centrosome indicates the area used for the colocalization analyses shown in Fig. 5E,F, Fig. S6C,D. An endosome-enriched ring corresponding to a 4.5 μm diameter circle around the centrosome, from which a 2 μm diameter circle (centrosomal area) was excluded, indicates the area used for the colocalization analyses shown in Fig. S6B. (D) Immunofluorescence analysis (IF) of CD3ζ and p-Tyr in conjugates of control (ctr) and BBS1KO (T KO) primary T cells with Raji B cells (APCs) in the absence of SAgs (n=3). Quantifications are shown in Fig. 2I, Fig. 3B. (E-G) Immunofluorescence analysis of p-ZAP-70 (E), p-LAT (F) and F-actin (G) in conjugates of control (ctr) and BBS1KD (J KD) Jurkat cells with Raji B cells (APCs) in the absence of SEE (n=3). Quantifications are shown in Fig. 3C,D, Fig. 5C. (H) Immunofluorescence analysis (IF) of control (ctr) and BBS1KD (J KD) Jurkat cells transfected with the LifeAct reporter and conjugated with Raji B cells (APCs) in the absence of SEE for 15 min (n=3). Quantifications are shown in Fig. 5D. Scale bar: 5 μm. Dashed lines indicate cell outlines.

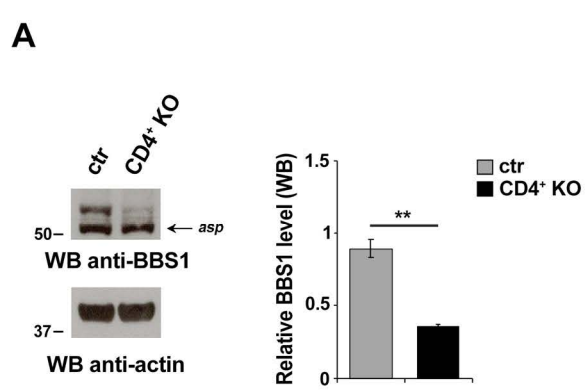

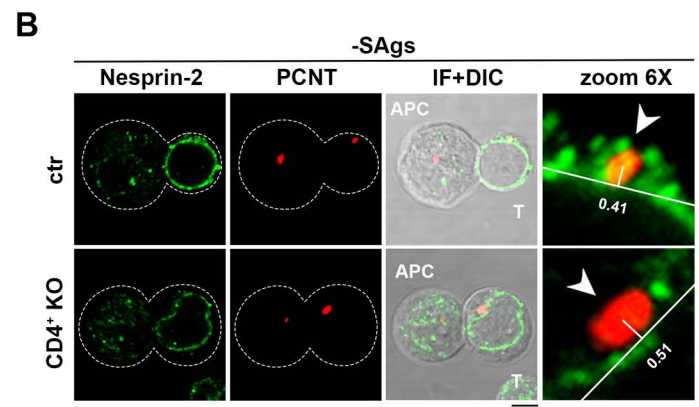

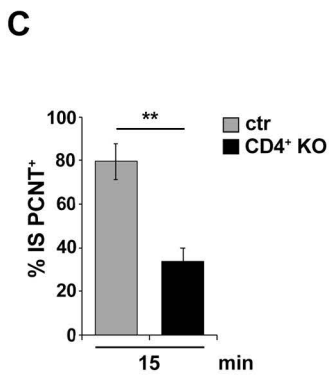

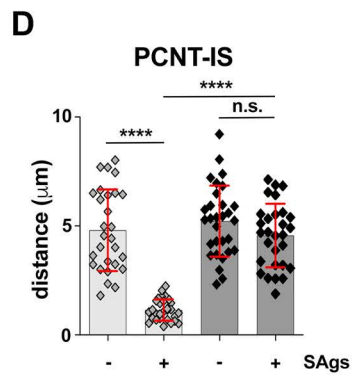

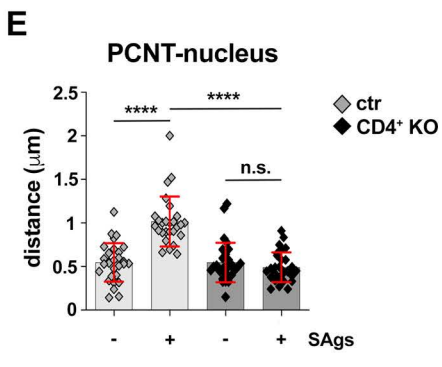

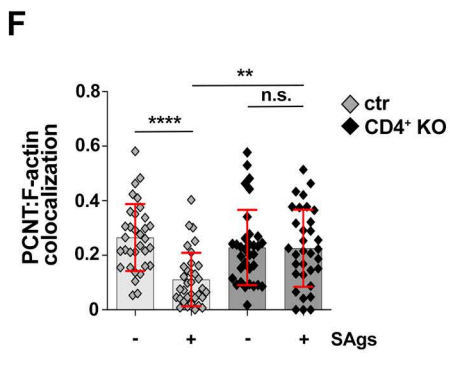

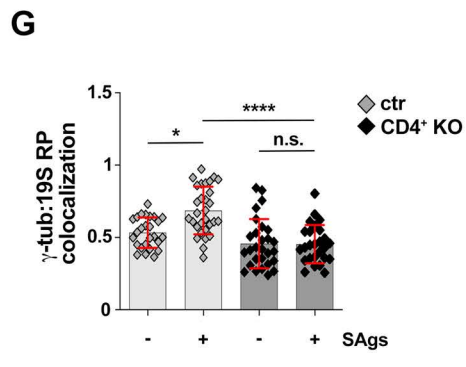

Fig. S5. BBS1-deficient CD4⁺ T cells form dysfunctional immune synapses. (A). Western blot (WB) analysis of BBS1 in lysates of control (ctr) and BBS1 KO (CD4⁺ KO) primary CD4⁺ T cells gene-edited by CRISPR-Cas9 technology. A representative immunoblot is shown. The migration of molecular mass markers is indicated (kDa). Right: Bar graph showing the relative protein expression normalized to actin (n=3, paired two-tailed Student's *t*-test). (B-E) Immunofluorescence analysis (IF) of 15-min conjugates of control (ctr) or BBS1 KO (CD4⁺ KO) primary CD4⁺ T cells with Raji cells (APCs) in the absence or presence of SAgs. Conjugates were co-stained for pericentrin (PCNT) and Nesprin-2. Representative images (medial optical sections) are shown in B. Boxes indicate the regions shown in 6X zoom images. Arrowheads indicate the centrosomes and the perpendicular lines show the centrosome-nucleus distances (see Fig. S4C for quantification). DIC, differential interference contrast. Quantification (percentage) of 15-min SAg-specific conjugates harboring PCNT staining at the IS (≥ 25 cells/sample, n=3, unpaired two-tailed Student's *t*-test) (C). Measurement of the distance (μm) of the centrosome (PCNT) from the T cell-APC contact site (D) (≥10 cells/sample, n=3, one-way ANOVA test) and from the nuclear membrane (Nesprin-2) (E) (≥10 cells/sample, n=3, Kruskal-Wallis test) in 15-min conjugates of control (ctr) and BBS1 KO (CD4⁺ KO) CD4⁺ T cells with Raji cells (APCs) in the absence or presence of SAgs. (F) Immunofluorescence analysis (IF) of centrosomal F-actin (phalloidin) in 15-min conjugates of control (ctr) or BBS1 KO (CD4⁺ KO) primary CD4⁺ T cells Raji cells (APCs) in the absence or presence of SAgs. Conjugates were co-stained for the centrosomal marker PCNT. Quantification using Manders' coefficient of the weighted colocalization of PCNT with centrosomal F-actin (see Fig. S4C for mask generation) (≥ 10 cells/sample, n=3, Kruskal-Wallis test). (G) Immunofluorescence analysis (IF) of 19S RP recruitment to the centrosome (γ–tub) in 1-min conjugates of control (ctr) or BBS1 KO (CD4⁺ KO) primary CD4⁺ T cells with Raji cells (APCs) in the absence or presence of SAgs. Quantification using Manders' coefficient of the weighted colocalization of 19S RP with the centrosome (γ–tubulin; γ–tub) (see Fig. S4C for mask generation) (≥ 10 cells/sample, n=3, Kruskal-Wallis test). Scale bar: 5 μm. Dashed lines in B indicate cell outlines. Data are expressed as mean±s.d. ****P≤0.0001; **P≤0.01; *P≤0.05; n.s., not significant.

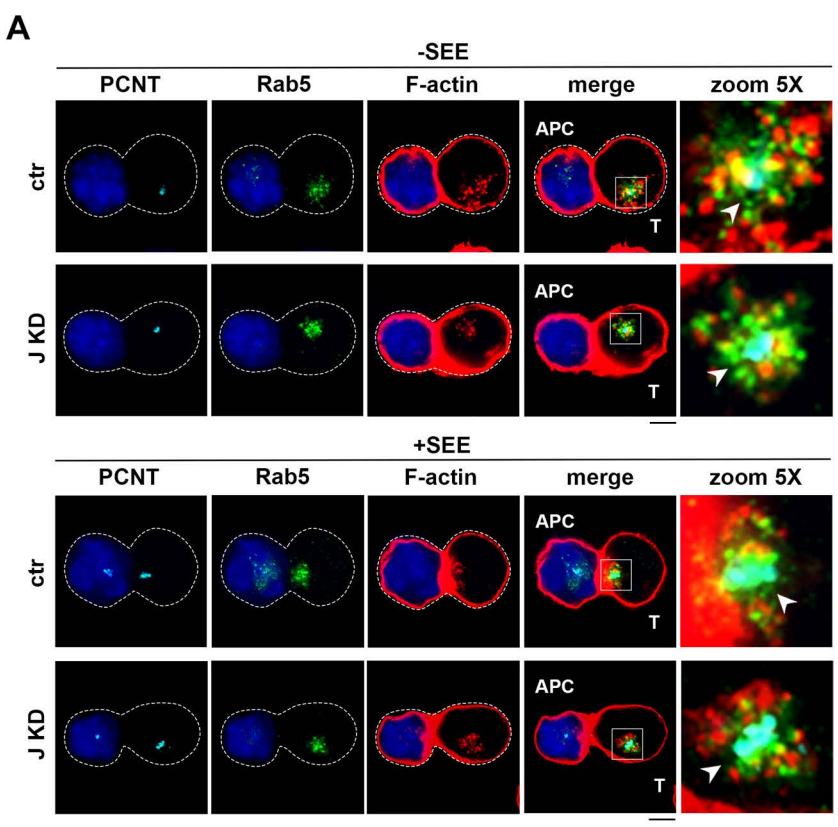

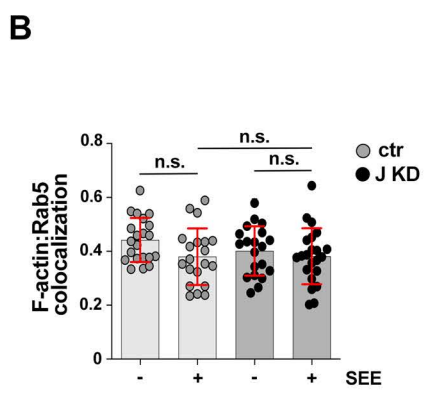

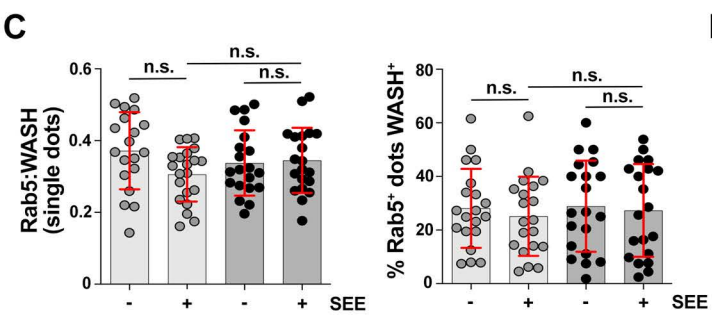

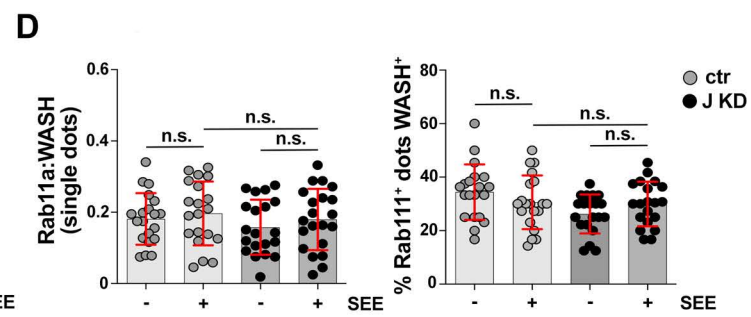

Fig. S6. BBS1 deficiency does not affect endosomal F-actin during IS assembly. (A) Immunofluorescence analysis (IF) of endosomal F-actin in control (ctr) or BBS1 KD (J KD) Jurkat cells conjugated with Raji cells (APCs) in the absence or presence of SEE for 15 min and triple stained for pericentrin (PCNT), Rab5 and F-actin. Representative images (medial optical sections) are shown. Dashed lines marks cell outlines. Arrowheads indicate the centrosomes. Boxes indicate the regions shown in 5X zoom images. DIC, differential interference contrast. (B) Colocalization analysis of F-actin with Rab5 in an endosome-enriched ring of 4.5 µm diameter around the PCNT-labelled centrosome, from which a 2 µm diameter circle (centrosomal area) was excluded (detailed in Fig. S4C) (≥10 cells/sample, n=2, one-way ANOVA test). (C,D) Immunofluorescence analysis (IF) of endosomal WASH in control (ctr) and BBS1KD (J KD) Jurkat cells conjugated with Raji cells (APCs) in the absence or presence of SEE for 15 min and co-stained for the endosomal markers Rab5 (C) and Rab11a (D) (see Fig. S4C for mask generation). Colocalization of WASH on individual dots (left) and quantification of $Rab5^+$ (C) or $Rab11a^+$ (D) dots positive for WASH (right) (≥10 cells/sample, 15 dots/cell, n=2, Kruskal Wallis test or one-way ANOVA based on normality distribution of different data sets). Scale bar: 5 µm. Data are expressed as mean±s.d. n.s., not significant.

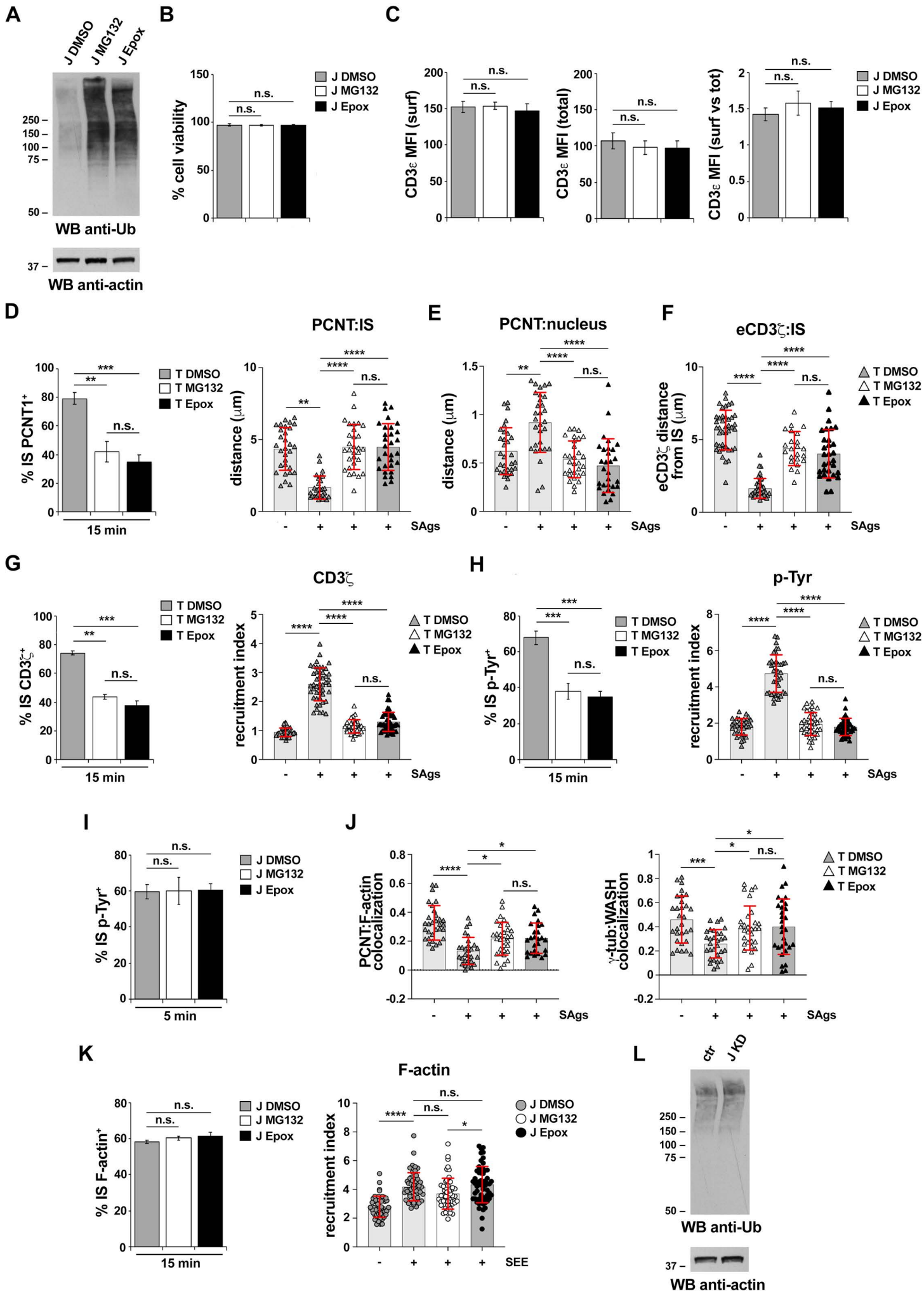

Fig. S7. Characterization of immune synapses formed by Jurkat and primary T cells treated with proteasome inhibitors. (A) Western blot (WB) analysis of ubiquitin (Ub) in lysates of control Jurkat cells pre-treated with carrier (dimethyl sulfoxide; DMSO), the proteasome inhibitors MG132 and epoxomicin (Epox) (n=3). Actin was used as loading control. (B) Viability (%) of control Jurkat cells pre-treated with carrier (J DMSO), MG132 (J MG132) or epoxomicin (J Epox) measured using Trypan Blue exclusion (n=3). (C) Flow cytometric analysis of CD3ε in control Jurkat cells pre-treated with carrier (J DMSO), MG132 (J MG132) or epoxomicin (J Epox), either intact (left) or permeabilized (middle) to quantify surface and total CD3ε, respectively. Data (mean±s.d.) are expressed as MFI in intact cells (surface) and permeabilized cells (total). The ratio of MFI of the surface and total pools is plotted on the histogram on the right (n=3, unpaired two-tailed Student's *t*-test). (D) Graphs: Quantification (percentage) of 15-min SAg-specific conjugates formed by primary T cells

pre-treated with carrier (T DMSO), MG132 (T MG132) or epoxomicin (T Epox) and showing PCNT staining at the IS (≥25 cells/sample, n=3, unpaired two-tailed Student's *t*-test) (left). Measurement of the distance (μm) of the centrosome (PCNT) from the T cell-APC contact site in primary T cells pre-treated with carrier (T DMSO), MG132 (T MG132) or epoxomicin (T Epox) and conjugated with Raji cells (APCs) in the absence or presence of SAgs for 15 min (≥ 10 cells/sample, n=3, Kruskal-Wallis test) (right). (E) Measurement of the centrosome-nucleus distance (μm) in primary T cells pre-treated with (T DMSO), MG132 (T MG132) or epoxomicin (T Epox) and conjugated with Raji cells in the absence or presence of SAgs for 15 min (see Fig. S4C for parameters used for quantification) (≥10 cells/sample, n=3, Kruskal-Wallis test). (F) Measurement of the distance (μm) of the endosomal TCR-CD3 pool (eCD3ζ) from the T cell-APC contact site in primary T cells pre-treated with carrier (T DMSO), MG132 (T MG132) or epoxomicin (T Epox) and conjugated with Raji cells (APCs) in the absence or presence of SAgs for 15 min (≥10 cells/sample, n=3, Kruskal-Wallis test). (G) Graphs: Quantification (percentage) of 15-min SAg-specific conjugates formed by primary T cells pre-treated with carrier (T DMSO), MG132 (T MG132) or epoxomicin (T Epox) and showing CD3ζ staining at the IS (≥25 cells/sample, n=3, unpaired two-tailed Student's *t*-test) (left). Relative CD3ζ fluorescence intensity at the IS primary T cells pre-treated with carrier (T DMSO), MG132 (T MG132) or epoxomicin (T Epox) and conjugated with Raji cells (APCs) in the absence or presence of SAgs for 15 min (≥10 cells/sample, n=3, Kruskal-Wallis test) (right). Data are expressed as recruitment index, which is calculated as the ratio of CD3ζ fluorescence intensity at the T cell-APC contact site to the total T cell area. (H) Graphs: Quantification (percentage) of 15-min SAg-specific conjugates formed by primary T cells, pre-treated with either carrier (T DMSO), MG132 (T MG132) or epoxomicin (T Epox) and showing p-Tyr staining at the IS (≥ 25 cells/sample, n=3, unpaired two-tailed Student's *t*-test) (left). Relative p-Tyr fluorescence intensity at the IS in primary T

cells pre-treated with carrier (T DMSO), MG132 (T MG132) or epoxomicin (T Epox) and conjugated with Raji cells (APCs) for 15 min in the absence or presence of SAgs for 15 min (≥10 cells/sample, n=3, Kruskal-Wallis test) (right). Data are expressed as recruitment index, which is calculated as the ratio of p-Tyr fluorescence intensity at the T cell-APC contact site to the total T cell area. (I) Quantification (percentage) of 5-min SEE-specific conjugates formed by control Jurkat cells pre-treated with carrier (J DMSO), MG132 (J MG132) or epoxomicin (J Epox) and showing p-Tyr staining at the IS (≥ 25 cells/sample, n=2, unpaired two-tailed Student's *t*-test). (J) Graphs: Quantification using Manders' coefficient of the weighted colocalization of PCNT with centrosomal F-actin (left) or γ–tub with centrosomal WASH (right) in primary T cells pre-treated with carrier (T DMSO), MG132 (T MG132) or epoxomicin (T Epox) and conjugated with Raji cells (APCs) in the absence or presence of SAgs for 15 min (see Fig. S4C for mask generation) (≥ 10 cells/sample, n=3, Kruskal-Wallis test). (K) Graphs: Quantification (%) of 15-min SEE-specific conjugates formed by control Jurkat cells pre-treated with carrier (J DMSO), MG132 (J MG132) or epoxomicin (J Epox) and showing F-actin staining at the IS (≥ 25 cells/sample, n=3, unpaired two-tailed Student's *t*-test) (left). Relative F-actin fluorescence intensity at the IS in Jurkat T cell pre-treated with carrier (J DMSO), MG132 (J MG132) or epoxomicin (J Epox) and conjugated with Raji cells in the absence or presence of SEE for 15 min (≥10 cells/sample, n=3, Kruskal-Wallis test) (right). Data are expressed as recruitment index, which is calculated as the ratio of F-actin fluorescence intensity at the T cell-APC contact site to the total T cell area. (L) Western blot (WB) analysis of ubiquitin (Ub) in lysates of control (ctr) and BBS1KD (J KD) Jurkat cells. Actin was used as loading control (n≥3). The migration of molecular mass markers is indicated (kDa). Data are expressed as mean±s.d. ****P≤0.0001; ***P≤0.001; **P≤0.01; *P≤0.05; n.s., not significant.

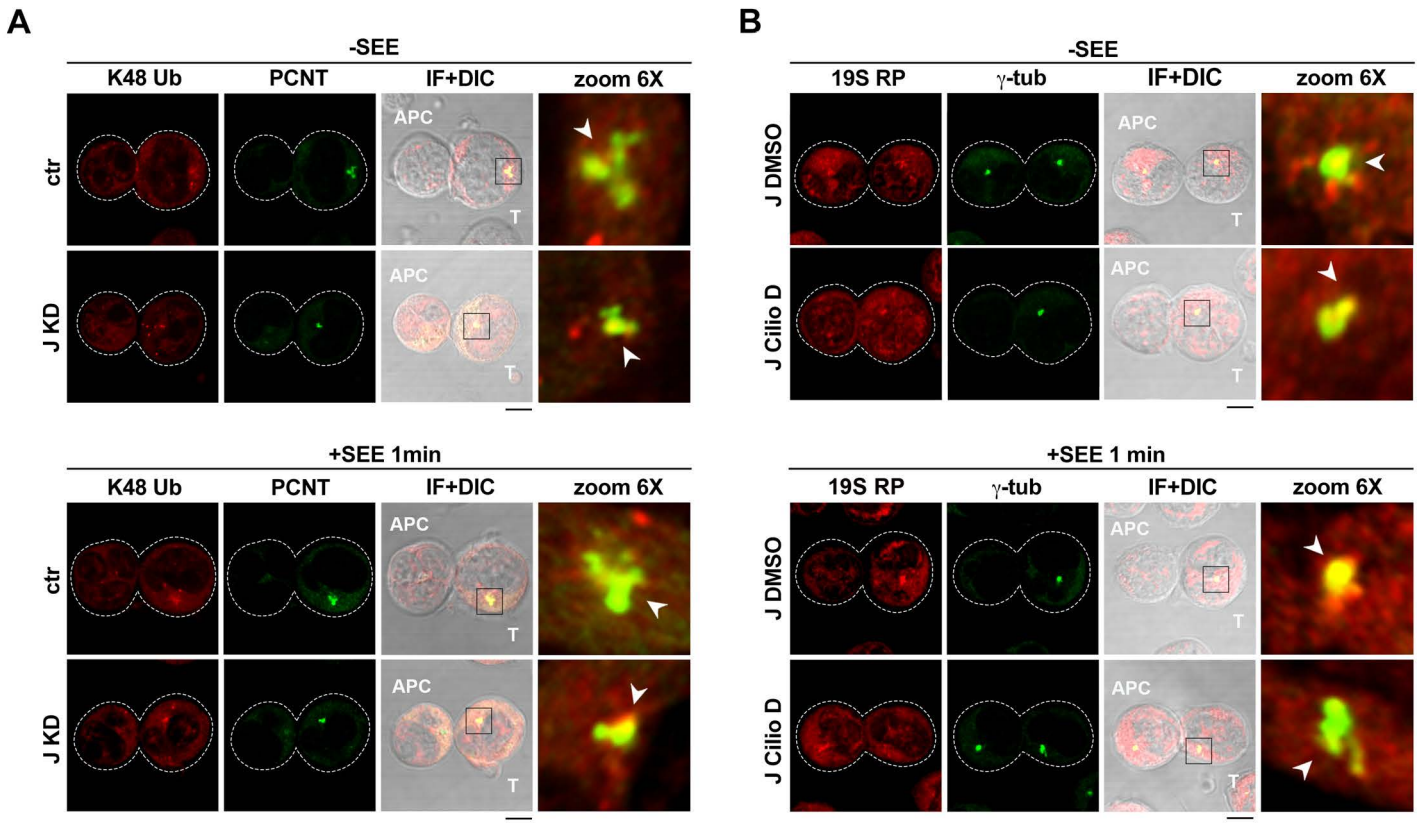

Fig. S8. Representative images of conjugates stained for K48 Ub and PCNT and of conjugates formed with ciliobrevin-treated T cells. (A). Representative images (medial optical sections) of K48-linked ubiquitin (K48 Ub) staining in 1-min conjugates of control (ctr) and BBS1KD (J KD) Jurkat cells with SEE-loaded or unloaded Raji cells (APCs) that had been seeded on poly-L-lysine-coated slides. Conjugates were co-stained for pericentrin (PCNT). Time course analysis of centrosomal K48 Ub is shown in Fig. 7D. (B) Representative images (medial optical sections) of 19S RP staining in 1-min conjugates of control Jurkat cells treated with either carrier (J DMSO) or 50 μM ciliobrevin D (J Cilio D) during conjugate formation with SEE-loaded or with unloaded Raji B cells seeded on poly-L-lysine-coated slides. Conjugates were co-stained for γ–tubulin (γ–tub). Quantification (percentage) of 15-min conjugates harboring γ–tub staining at the IS formed by Jurkat cells treated either with carrier (J DMSO) or Cilio D (J Cilio D) and harboring γ–tub staining at the IS was 65±4 and 25±5 (media±s.d.), respectively. Quantification of the centrosomal 19S RP at different time points is shown in Fig. 7G. Arrowheads indicate the centrosomes. Boxes indicate the regions shown in 6X zoom images. DIC, differential interference contrast. Scale bar: 5 μm. Dashed lines mark cell outlines.

Table S1. List of the primers used in this study

Oligo name	Sequence	Description
common reverse primer	AGCACCGACTCGGTGCCACT	gRNA production
GFP gRNA	ttaatacgactcactataggGGGCGAGGAG CTGTTCACCGgttttagagctagaaatagc	gRNA production
BBS1 gRNA	ttaatacgactcactataggGGATGCGCAC TACGACCCAAgttttagagctagaaatagc	gRNA production
BBS1 gRNA1	GGATGCGCACTACGACCCAA	gRNA sequence cloned into pSpCas9(BB)-2A-GFP plasmid
BBS1 gRNA2	GGGCTTTCGGTCATCACCAG	gRNA sequence cloned into pSpCas9(BB)-2A-GFP plasmid
BBS1 fw	AATTCGAAGTGGTTGGATGC	qPCR primer
BBS1 rv	ATGTTGCTCCATGAGGAAGG	qPCR primer
BBS2 fw	TTCCCCTCTTGCGATTATTG	qPCR primer
BBS2 rv	GTCACACAAGGCCAAGGAAT	qPCR primer
BBS4 fw	ACCACTTCAACCAGCAAACC	qPCR primer
BBS4 rv	GGCTTTGTGAACTGGGATGT	qPCR primer
BBS5 fw	CGGATGCTTTTGTGGCTTAT	qPCR primer
BBS5 rv	CCAAAGTCCCTGTAGGGTGA	qPCR primer
BBS7 fw	CCAGTACGCAAGTGGGAAAT	qPCR primer
BBS7 rv	CTTCCACCATTCCGTCATCT	qPCR primer
BBS8 fw	AGAGGCAGCTGATGTCTGGT	qPCR primer
BBS8 rv	GCGTGGTTGTTGTTGTTGAC	qPCR primer
BBS9 fw	CCCCACATTCCTGTAGCAGT	qPCR primer
BBS9 rv	AGAAGGATCTGTCCCCAGGT	qPCR primer
BBS18 fw	ACCATCTCGACTCACTGCAA	qPCR primer
BBS18 rv	TGAGATTTAAGGGCTGGGCA	qPCR primer
HPRT1 fw	AGATGGTCAAGGTCGCAAG	qPCR primer
HPRT1 rv	GTATTCATTATAGTCAAGGGCATATC	qPCR primer

Table S2. List of the antibodies used in this study

Antibody	Host Species	Cat.No.	Source	Dilution WB	Dilution IF	Dilution FC
AF555 phalloidin		A34055	Invitrogen	-	1:100 1:50	-
anti-actin	mouse	MAB1501	Merck - Life Science	1:10000	-	-
anti-BBS1	rabbit	ab166613	AbCam	1:1000	-	-
PE anti-CD3ε	mouse	317308	BioLegend	-	-	1:100
anti-CD3ζ	mouse	sc-1239	Santa Cruz	-	1:30	-
anti-CEP131	rabbit	ab99379	AbCam	-	1:300	-
anti-CEP290	rabbit	ab84870	AbCam	-	1:300	-
anti-dynein	mouse	MAB1618	Merck - Life Science	1:500	-	-
anti-GM130	mouse	610822	BD	-	1:100	-
anti-GFP	mouse	A11120	Invitrogen	-	1:200	-
anti-GFP	rabbit	A11122	Invitrogen	1:1000	1:200	-
anti-Nesprin-2	mouse	NBP2-59944	Novus	-	1:50	-
anti-p-Tyr	mouse	05-1050	Merck - Life Science	-	1:100	1:400
anti-p-Tyr	rabbit	8954	Cell Signaling	-	1:100	-
anti-p-LAT	rabbit	3584	Cell Signaling	-	1:50	-
Anti-p-ZAP70	rabbit	2701	Cell Signaling	-	1:50	-
Anti-PCM1	mouse	sc-398365	Santa Cruz	-	1:400	-
anti-PCNT	rabbit	ab4448	AbCam	-	1:200	-
anti-Rab5	mouse	610724	BD Biosciences	-	1:50	-
anti-Rab7a	mouse	sc-376362	Santa Cruz	-	1:50	-
anti-Rab11a	rabbit	2413	Cell Signaling	-	1:50	-
Anti-RFP	rabbit	600-401-379	Rockland Immunochemicals	-	1:500	-
anti-γ-tubulin	mouse	T6557	Merck - Life Science	1:5000	1:200	-
anti-β-tubulin	rabbit	15115	Cell Signaling	1:2000	-	-

anti-Ub	mouse	3936	Cell Signaling	1:500	-	-
anti-Ub	mouse	04-263	Merck - Life Science	-	1:50	-
anti-K48 Ub	rabbit	05-1307	Merck - Life Science	-	1:50	-
Anti-WASH1	mouse	SAB42 00552	Merck - Life Science	-	1:100	-
anti-WASH1	rabbit	PA5-51731	Invitrogen	1:500	1:100	-
anti-19S RP	rabbit	ab140450	AbCam	1:2000	-	-
anti-19S RP	rabbit	ab3317	AbCam	-	1:100	-